Geophys. J. Int. (2007) **169,** 1043–1068 doi: 10.1111/j.1365-246X.2006.03259.x

New insights into the lithosphere beneath the Superior Province from Rayleigh wave dispersion and receiver function analysis

Fiona A. Darbyshire,[1,2*] David W. Eaton,[1] Andrew W. Frederiksen[3] and Leila Ertolahti[1]

[1]*Department of Earth Sciences, University of Western Ontario,* 1151 *Richmond Street London, ON* N6A 5B7, *Canada.*
E-mail: fiona@olympus.geotop.uqam.ca.
[2]*Geological Survey of Canada;* 615 *Booth Street rm* 216, *Ottawa, ON* K1A 0E9, *Canada*
[3]*Department of Geological Sciences, University of Manitoba, Winnipeg, MB* R3T 2N2, *Canada*

Accepted 2006 October 6. Received 2006 September 20; in original form 2006 May 9

SUMMARY

We present new models of shear wave velocity structure of the lithosphere and upper mantle beneath northern and eastern Ontario and surrounding regions. The study area is dominated by the Archean Superior Province, with Proterozoic orogenic belts to the south and southeast. Over the course of ∼3 Ga, the region has been shaped by accretionary and orogenic events, periods of rifting and the influence of a number of mantle hotspots.

New data from the broad-band POLARIS/FedNor seismic network, along with permanent stations of the Canadian National Seismograph Network, are used for a seismic study of the crust and upper mantle beneath the region. This article concentrates primarily on a study of the upper mantle, carried out using two-station phase velocity analysis of teleseismic Rayleigh waves. Dispersion curves were measured for 100 two-station paths across the region, of which 30 were analysed to give 1-D path-averaged models of shear wave velocity structure. Dispersion measurements yielded phase velocity data for periods from ∼25 to ∼170 s, allowing us to resolve shear wave velocities to a depth of ∼300 km. The dispersion curves indicate an upper-mantle structure broadly characteristic of continental shield regions, but there are significant variations in the properties of the data across the province.

In the central and western Superior Province, inferred lithospheric thicknesses vary between approximately 140 and 200 km. In general, the models are characterized by a well-developed 'lid' of high-velocity mantle underlain by a zone of reduced velocity. The highest lid velocities are modelled along a path whose azimuth corresponds to the fast direction of anisotropy resolved through *SKS* splitting analysis. The far northeast of Ontario has the thickest (∼220–240 km) lithospheric lid. Eastern Ontario has a complex structure that gives rise to a large variation in the structures modelled from the two-station paths. Apparent lithospheric thicknesses range from ∼100 to ∼220 km. This large variation is interpreted to arise from highly heterogeneous mantle structure and/or anisotropy across the Abitibi Greenstone Belt, the Southern Province, and the Proterozoic Grenville Province.

Receiver function analysis shows variations in Moho depth and bulk Poisson's Ratio in the Superior Province crust. The crustal thickness varies from ∼34 to ∼44 km through most of the province, with a zone of anomalously thick crust (48 km) in the Kapuskasing Structural Zone region. Measurements of bulk Poisson's Ratio indicate that the crust is highly felsic in some parts of the province, but includes a significant mafic component in parts of the western Superior and eastern Ontario, regions that have been affected by uplift or rifting.

*Now at: GEOTOP-UQAM-McGill, Département des Sciences de la Terre et de l'Atmosphère, Université du Québec à Montréal, CP 8888 succursale Centre-Ville, Montréal, QC, H3C 3P8, Canada.

The new results, together with information from other recent studies of shear wave splitting and body-wave tomography, show that the Superior craton is far from a homogeneous entity. Rather it is divisible, on the basis of thickness, anisotropy and velocity structure of the crust and lithosphere, into distinct subdomains that reflect the complex tectonic history of this region. The large range of inferred thicknesses of the crust (34–48 km) and lithosphere (100–240 km) within the Superior craton represents a significantly greater variability than has been previously observed for Archean lithosphere.

Key words: crustal thickness, FedNor, lithosphere, POLARIS, Rayleigh wave dispersion, receiver functions, Superior craton .

1 INTRODUCTION

Cratons constitute interior parts of continents that have remained tectonically quiescent over a billion-year timescale (Hoffman 1988). They owe their long-term preservation to the presence of refractory and cold, yet buoyant, lithospheric roots composed of highly melt-depleted peridotitic mantle (e.g. Jordan 1975; Griffin *et al.* 1999; Carlson *et al.* 2005) that have remained convectively isolated from the asthenosphere (Pearson 1999; Forte & Perry 2000). In global seismic tomographic studies (e.g. Su & Dziewonski 1994; Li & Romanowicz 1996; Masters *et al.* 1996; Shapiro & Ritzwoller 2002; Nettles & Dziewonski 2004), these lithospheric roots beneath cratons are manifested as high-velocity mantle 'lids' that extend to depths of ∼150–300 km. Continental-scale surface wave inversions (e.g. Debayle & Kennett 2000; Godey *et al.* 2004; van der Lee & Frederiksen 2005) provide better-resolved seismic images of cratonic mantle roots than global studies but still do not provide sufficient detail to discriminate between different models for their formation (Griffin *et al.* 1999).

Here we use data from the recently deployed POLARIS and FedNor broad-band seismograph arrays to probe the lithospheric structure of a large part of the southern Canadian Shield, north of the Great Lakes (Fig. 1). The study area is broadly underlain by a vast high-velocity mantle lid in global tomographic models, and is dominated by the Superior Province, the largest Archean craton in the world (Thurston *et al.* 1991). The study region is bordered to the north and south by Proterozoic orogenic belts and has experienced a complex tectonic history, with influences from large-scale rifting and plume-related events over a time span of ∼3 billion years. The objectives of this paper are to use mantle velocity structure inferred from Rayleigh wave dispersion analysis, coupled with *SKS* splitting studies and crustal thickness determinations from receiver functions, to examine the seismic characteristics of the craton with a higher resolution than has previously been possible.

1.1 Geological and tectonic summary

A summary of the major tectonic events that have shaped the study region is given in Table 1.

The Superior Province is the world's largest Archean craton, with an area of ∼1.6 million km^2 (Thurston *et al.* 1991). The central and western parts of the Superior craton investigated here are largely composed of roughly eastwest trending subprovinces (e.g. Thurston *et al.* 1991; Percival 1996; Ludden & Hynes 2000). These subprovinces can be divided geologically into granite-greenstone belts, metasedimentary gneisses, high-grade gneisses and plutonic complexes. The craton was assembled over a period of time from ∼3 to ∼2.6 Ga, by a progressive accretion from the south of magmatic arc complexes (e.g. Thurston *et al.* 1991; Calvert *et al.* 1995; Percival 1996). The culminating event in the assembly of the Superior Province was the ∼2.8–2.6 Ga Kenoran orogeny. The Superior subprovinces include the Abitibi Greenstone Belt, which is the largest of the world's granite-greenstone belts (Thurston *et al.* 1991). Paleoproterozoic metasediments outcrop on the southern and eastern parts of the craton (the Southern Province), with ages of ∼2.2 Ga.

Proterozoic orogenic belts bound the Superior Province. The ∼1.8 Ga Trans-Hudson Orogen outcrops to the northwest of the study area (e.g. Hoffman 1988), but is obscured to the north by Phanerozoic platform sediments, aside from the Sutton Inlier outcrop (see station SILO; Fig. 1). The Penokean Orogen (∼1.9–1.6 Ga; Ludden & Hynes 2000) bounds the province to the south. The younger Grenville Orogen (∼1.1–1.0 Ga; Thurston *et al.* 1991; Ludden & Hynes 2000) is the major influence on the geology of southeastern Ontario and southwestern Quebec.

The Grenville Orogen is the end result of a continuous continent-continent collision, which began with the earlier Penokean Orogeny. It is a complex region of reworked rocks from the Superior and Southern provinces and the Penokean fold belt, and Mezoproterozoic supracrustal and plutonic rocks, generally younging to the southeast (e.g. Davidson 1996; Ludden & Hynes 2000). The Grenville Province formed the southeast limit of Proterozoic Laurentia, accreting onto the Laurentian margin through a series of magmatic arcs and backarc material (Rivers 1997). The Superior-Grenville margin is complex, with indications of wedging of lithospheric material within the northern Grenville Province (e.g. Rivers 1997; Rondenay *et al.* 2000b).

In the north of Ontario, the rocks of the Superior Province are unconformably overlain by the Phanerozoic platform sediments of the Hudson Bay and James Bay Lowlands, associated with the Hudson Bay and Moose River intracratonic basins.

Major rifting and faulting events have had a considerable influence on the south and central regions of the Superior Province. The Kapuskasing Structural Zone is a major thrust fault that has uplifted and exposed a large section of Archean lower crustal rocks along a ∼800 km length trending southwest to northeast. The structure is characterized by thickened crust, a positive gravity signature and aeromagnetic anomalies (Percival & West 1994, and references therein). The history of the Kapuskasing Structural Zone is not well constrained, but it is thought (Percival & West 1994) that the major part of the uplift occurred in response to stresses transmitted into the craton interior from plate collisions and orogenic events at ∼1.9 Ga. At ∼1.11–1.09 Ga, the region was affected by the Keweenawan Mid-continent Rift, thought to have resulted in the world's largest plateau basalt eruption (Thurston *et al.* 1991). In the Lake Superior region, extending northward to the Nipigon region (between stations LDIO and NANO on Fig. 1), the failed rifting event resulted in emplacement of flood basalts with thickness of up to 30 km, with related igneous rocks and metasediments. In the southeast, the Ottawa-Bonnechere Graben opened in the late Proterozoic—early

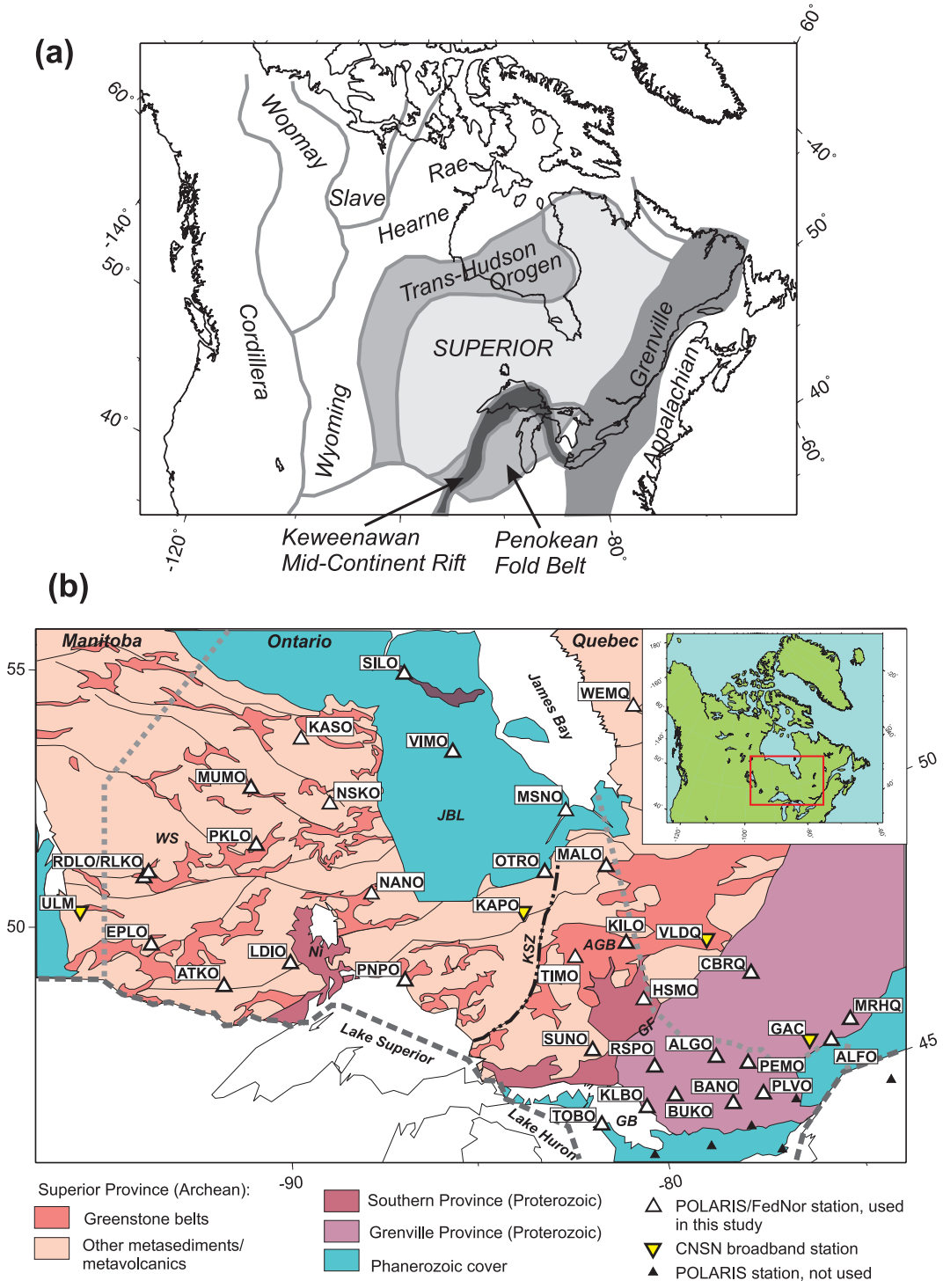

Figure 1. (a) Simplified tectonic map of Canada and the northern USA, showing the positions of the major tectonic provinces. (b) Map of the study region (Ontario, westernmost Quebec and eastern Manitoba, north of 45°N), showing major geological features and the locations of seismograph stations used in the analysis. POLARIS/FedNor stations are shown as white triangles; the yellow inverted triangles denote permanent broad-band CNSN (Canadian National Seismograph Network) stations. WS—Western Superior; JBL—James Bay Lowlands; KSZ—Kapuskasing Structural Zone; AGB—Abitibi Greenstone Belt; GF—Grenville Front; GB—Georgian Bay; Ni—Lake Nipigon region.

Cambrian, and is thought to represent a failed rifting arm developed at the onset of Laurentian breakup (e.g. Kamo *et al.* 1995). The northward extension to this graben system is the Lake Timiskaming Structural Zone, a set of faults lying along the Ontario–Quebec border in eastern Ontario, which is still seismically active today (Adams & Basham 1991).

1.1.1 Plumes and rifts

Evidence for Precambrian plume influences on the northeastern Ontario Shield can be found through examination of large dyke swarms (e.g. Ernst & Buchan 2001). The oldest of these is the Matachewan dyke swarm, centred on southeastern Georgian Bay (close to station

Table 1. Summary of major geological/tectonic events shaping the study region, as described in detail in the text.

Date	Event
3–2.6 Ga	Assembly of Superior Craton
2.8–2.6 Ga	Kenoran Orogen completes assembly process
2.49–2.45 Ga	Hotspot influence and rifting on SE Superior margin leads to emplacement of Matachewan dyke swarm
2.2 Ga	Age of Southern Province; Nipissing Sills fed by distant Ungava plume
1.9–1.6 Ga	Penokean Orogen on southern margin of Superior Province; likely age of major uplift in Kapuskasing Structural Zone
∼1.8 Ga	Trans-Hudson Orogen on northwest Superior margin
∼1.1 Ga	Keweenawan Mid-Continent Rift on southern Superior margin
1.1–1.0 Ga	Grenville Orogen on southeast Superior margin
Late Proterozoic - Early Cambrian	Opening of Ottawa-Bonnechere Graben and Lake Timiskaming structural zone (Ontario/Quebec border region)
Phanerozoic	Development of Hudson Bay and Moose River intracratonic basins
180–134 Ma	Emplacement of kimberlites along track of Great Meteor hotspot

KLBO, Fig. 1), dated at 2.49–2.45 Ga and thought to be associated with a rifting/breakup event on the southeastern Superior margin. The Nipissing Sills within the Southern Province may have been fed by the ∼2.2 Ga Ungava plume, ∼1400 km to the northeast. A dyke swarm in the Sudbury region (close to station SUNO, Fig. 1) is dated at ∼1.24 Ga. The emplacement of dyke swarms has been linked with the stabilization of continental lithosphere (Nelson 1991).

The region has also been affected by plume activity in more recent times, with the inferred passage under eastern North America of the Great Meteor hotspot (Crough 1981; Sleep 1991; Heaman & Kjarsgaard 2000), likely associated with the Mesozoic opening of the North Atlantic Ocean. Evidence for the passage of the hotspot comes from epeirogenic uplift (Crough 1981), alkaline (Sleep 1991) and kimberlitic (Heaman & Kjarsgaard 2000) volcanic products progressively younging to the southeast, and mantle velocity anomalies (Rondenay *et al.* 2000a; Aktas & Eaton 2006). In the present study area, a trend of kimberlites extends from the Attawapiskat kimberlite cluster in the north (close to station VIMO; Fig. 1) to the Kirkland Lake cluster (south of station KILO) and the Timiskaming cluster (close to station HSMO). The small-volume kimberlitic melts, as opposed to large-scale basaltic melting, are thought to indicate that the plume passed beneath thick (at least 150 km) continental lithosphere (e.g. Thompson & Gibson 1991).

1.2 Previous geophysical studies

The crust and uppermost mantle beneath northern and eastern Ontario have been studied using seismic reflection and refraction methods, through the Canada-wide Lithoprobe project (*www.lithoprobe.ca*). Four of the major transects are of interest to this study: Western Superior, Kapuskasing Structural Zone, Abitibi-Grenville and Great Lakes International Multidisciplinary Program on Crustal Evolution (GLIMPCE).

The crust and uppermost mantle structure of the Western Superior Province was investigated in detail by Musacchio *et al.* (2004), using data from two orthogonal ∼600 km long refraction/wide-angle reflection profiles. They modelled a layered crust of thickness ∼32–45 km, with significant variations in the properties of the lower crust and uppermost mantle. A high-velocity, anisotropic layer '2S' at the base of the crust in the southern part of the study region was interpreted as a slab of remnant oceanic crust whose northsouth lineation was imposed during tectonic accretion. In the mantle, a northward-dipping high-velocity layer with significant anisotropy and an approximately eastwest fast direction was imaged. This layer was interpreted as a relict slab of oceanic lithosphere, accreted during the final stages of Western Superior lithospheric assembly.

Refraction seismic studies of the Kapuskasing Structural Zone (Boland & Ellis 1989; Percival & West 1994) indicate anomalously high velocities in the upper-to-middle crust, suggesting uplift of lower-crustal material. The Moho is significantly deeper than the surrounding region, with a crustal thickness reaching over 50 km in places. High seismic velocities (∼7.2–7.8 km s^{-1}) are modelled in the lower crust between ∼30 and ∼50 km depth. The crust–mantle boundary is believed to be complex in nature.

Across a northsouth transect in the Abitibi-Grenville region, the Moho depth varies between 35 and 45 km (Ludden & Hynes 2000). It is at its shallowest beneath the Grenville Front and close to the mantle-ward extension of the dipping Grenville Front tectonic zone (Eaton *et al.* 2006). Beneath the Grenville Province, the crustal thickness increases southward, from ∼40 to ∼45 km. The crust beneath the Abitibi subprovince varies from 37 to 40 km. Reflection seismic data show signs of dipping reflectors extending through the entire crustal column into the mantle; the reflectors are strongest at the northern end of the Abitibi greenstone belt. Changes in reflectivity patterns beneath the Abitibi subprovince are thought to represent the presence of mafic underplating (e.g. Ludden & Hynes 2000).

Teleseismic studies of the Western Superior were carried out in 1989, using a deployment of intermediate-period seismographs along a northsouth line close to the Ontario-Manitoba border in Canada, and extending southwest into the USA. The APT89 experiment (Silver *et al.* 1993) primarily used shear wave splitting analysis (Silver & Kaneshima 1993) and *P*- and *S*-wave traveltime delays (Bokelmann & Silver 2000) to characterize the nature of the upper mantle beneath the transect. In the Canadian Western Superior, significant ENE-trending shear wave splitting was observed, with delay times close to 2 s in the central part of the region. Large negative *S*-wave traveltime residuals were also measured in this region, but little variation in *P*-wave residual was observed. The authors interpreted the measurements as resulting from a thick, cold lithospheric mantle with significant 'frozen' anisotropy.

A more recent experiment was carried out using a 480 km line of broad-band seismometers deployed in 1997, on a roughly northsouth line ∼200 km east of the APT89 array. The structure and anisotropy of the region were investigated using *SKS* splitting (Kay *et al.* 1999a), traveltime tomography (Sol *et al.* 2002) and surface

wave analysis (Kendall *et al.* 2002; Sol 2003). Large *SKS* splits with delay times of 1.1–2.1 s and fast directions approximately aligned with regional geological boundaries and apparent plate motion were resolved. Traveltime tomography showed a dipping high-velocity anomaly, interpreted by the authors as a relict subducting slab, and two low-velocity anomalies. The shallower anomaly was interpreted as being associated with dehydration at the edge of a downwelling slab, whereas the deeper anomaly was thought to represent the effect of later upwelling in the mantle. Mantle models from sets of two-station surface wave dispersion measurements showed a high-velocity upper mantle, and further evidence for significant mantle anisotropy was gained from measurements of Rayleigh-Love wave velocity discrepancy, the dependence of the dispersion curves on path orientation, and measurements of surface wave particle motion.

The mantle structure beneath the Abitibi-Grenville region was studied in detail by Rondenay *et al.* (2000a,b) using a temporary deployment of densely spaced broad-band seismographs (the Abi-96 deployment) placed in a roughly northsouth line. They investigated crust and upper-mantle structure using receiver function analysis, shear wave splitting and traveltime tomography. A Moho depth of 35–45 km was resolved along the array, with indications of a tectonic wedge beneath the Moho. *SKS* splitting analysis yielded moderate (∼0.6 s) splits along the array, with fast directions ranging between WNW–ESE and WSW–ENE. Traveltime tomography indicated a prominent (∼1 per cent *P*-wave slowness relative to the region of study) steeply dipping low-velocity anomaly in the upper mantle (∼50–300 km depth), which the authors related to a possible northward extrapolation of the Monteregian-White Mountain-New England Seamount track, associated with the Great Meteor hotspot. The low-velocity anomaly is surrounded by higher than average velocities, likely corresponding to a thick lithospheric root beneath the region.

A more recent traveltime tomography study by Aktas & Eaton (2006) used data from the POLARIS network (Eaton *et al.* 2005) in southern and eastern Ontario plus traveltimes from the Abi-96 profile described in the previous paragraph. They imaged a low-velocity region, interpreted as alteration associated with the interaction of the Great Meteor hotspot with the lithosphere, and a linear northeast-striking high-velocity anomaly, interpreted as a possible relict subducting slab.

The anisotropy beneath the Grenville and Southern provinces in eastern Ontario, and the Abitibi greenstone belt, was investigated by Eaton *et al.* (2004) and Frederiksen *et al.* (2006a) using both *SKS* splitting analysis and magnetotelluric measurements. They found that the average anisotropy for the region lies in an eastwest direction, broadly consistent with average plate motion. However, some significant spatial variation also exists, with some correlation to major tectonic boundaries, and there is evidence for anisotropy in the crust, the mantle lithosphere and the asthenosphere. The largest splits for the region occur in the southeast, where continental-scale tomographic studies image anomalously low shear wave velocity (van der Lee & Frederiksen 2005). Receiver function analysis at station GAC suggests the presence of multiple anisotropic layering in the uppermost mantle.

Body-wave tomography has been carried out for northern and eastern Ontario by Frederiksen *et al*.(2006b). The tomographic images show higher than average velocities throughout much of the western Superior, a linear trend of lower than average velocities in eastern Ontario, and possible regions of lowered velocity in central-northern Ontario. The new model places previous local-scale studies into a broader regional context, highlighting the major differences between the west and east Superior Province, and the Grenville Province to the southeast.

A large-scale magnetotelluric investigation of the western Superior Province was carried out by Ferguson *et al.* (2005). They found highly resistive crust beneath the oldest terranes, with more conductive crust to the south, and an eastwest trending conductivity anomaly between the oldest terrane and the Neoarchean terranes accreted to the south. The mantle lithosphere was found to be relatively conductive beneath the oldest terranes. In the Nipigon region, which has been significantly affected by the Mid-continent Rift, anomalously high resistivity was measured for both the crust and uppermost mantle. Long-period geoelectric strikes were generally aligned with the eastwest trending subprovince boundaries, suggesting that most of the western Superior Province has undergone little significant deformation or heating since the province was assembled.

1.2.1 Global and continental-scale studies

Global tomographic models (e.g. Su & Dziewonski 1994; Li & Romanowicz 1996; Masters *et al.* 1996; Nettles & Dziewonski 2004; Ritsema *et al.* 2004) indicate a significant high-velocity anomaly across much of North America, centred on central-northern Canada. The depth extent of the anomaly varies depending on the model parameters and the shear wave polarization considered, but is typically ∼200–250 km for models based on S_V-structure. In general, little internal structure can be resolved within the high-velocity anomaly for most global tomography results.

The global surface wave study of Shapiro & Ritzwoller (2002) gives more detail to the shear wave velocity models. In this case, the high-velocity anomaly covers almost all of Ontario to a depth of at least 150 km, with the exception of a region of relatively lower velocities (<1.5 per cent above the reference model) covering southeastern Ontario. Below 150 km depth, the extent of the high-velocity anomaly is more restricted, confined to the northern half of Ontario and north-central USA. At 250 km depth, there is little evidence for high shear wave velocities beneath the region; instead, a low-velocity anomaly is modelled beneath westernmost Quebec.

Continental-scale shear wave velocity models of North America (e.g. Godey *et al.* 2004; van der Lee & Frederiksen 2005) also show a significant high-velocity anomaly beneath most of Canada. High mantle velocities are apparent beneath Ontario to depths of at least 200 km, except for an indentation into the high velocity lithospheric root beneath North America, which extends into the Great Lakes region.

1.3 The POLARIS/FedNor seismograph network

This study primarily uses teleseismic data recorded by a network of temporary seismograph stations in northern and eastern Ontario and western Quebec (Table 2). The stations were deployed over a period of 4 yr, starting in summer 2002, as part of the POLARIS (Portable Observatories for Lithospheric Analysis and Research Investigating Seismicity) project (Eaton *et al.* 2005). Stations in northern Ontario that extend the POLARIS network were deployed using funding from FedNor (the Federal Economic Development Initiative for Northern Ontario). Each station consists of a Nanometrics Trident digitizer and Libra VSAT communications system, with a broad-band Guralp CMG-3ESP or CMG-3T seismometer (though some stations were equipped with CMG-40T sensors for their first year of deployment). The stations are self-reliant, using batteries

Table 2. Permanent and temporary broad-band seismograph stations used in this study. POLARIS—Portable Observatories for Lithospheric Analysis and Research Investigating Seismicity (southeast Ontario/southwest Quebec network; see Acknowledgments for funding details). FedNor—Federal Economic Development Initiative for Northern Ontario. GSC-NRD—Geological Survey of Canada, Northern Resources Development programme. CNSN—Canadian National Seismograph Network. All stations are in Ontario unless stated otherwise. All stations except the CNSN stations are affiliated to the POLARIS project. Negative longitudes represent degrees West.

Station	Location	Latitude	Longitude	Affiliation	Deployment
ALFO	Alfred	45.6283	−74.8842	POLARIS	2003/10/02–present
ALGO	Algonquin Provincial Park	45.9544	−78.0509	POLARIS	2002/09/11–present
ATKO	Atikokan Mine	48.8231	−91.6005	FedNor/GSC-NRD	2004/06/09–present
BANO	Bancroft	45.0198	−77.9280	POLARIS	2002/08/25–present
BUKO	Buck Lake	45.4423	−79.3990	POLARIS	2003/11/02–present
CBRQ	Cabonga Reservoir, Quebec	47.3092	−76.4707	POLARIS	2004/07/30–2005/05/19
EPLO	Experimental Lakes	49.6737	−93.7258	FedNor/GSC-NRD	2004/06/11–present
HSMO	Cobalt	47.3708	−79.6657	FedNor/GSC-NRD	2005/07/20–present
KASO	Kasabonika Lake	53.5279	−88.6414	FedNor/GSC-NRD	2005/08/03–present
KILO	Kirkland Lake	48.4972	−79.7232	FedNor/GSC-NRD	2003/06/22–present
KLBO	Killbear Provincial Park	45.3566	−80.2132	POLARIS	2003/07/28–present
LDIO	Lac des Isle Mine	49.1750	−89.5955	FedNor/GSC-NRD	2004/06/16–present
MALO	McAlpine Lake	50.0244	−79.7635	FedNor/GSC-NRD	2003/06/20–present
MRHQ	Morin Heights, Quebec	45.8870	−74.2127	POLARIS	2004/08/07–present
MSNO	Moosonee	51.2913	−80.6113	FedNor/GSC-NRD	2005/07/23–present
MUMO	Musselwhite Mine	52.6128	−90.3914	FedNor/GSC-NRD	2003/06/15–present
NANO	Aroland	50.3543	−86.9684	FedNor/GSC-NRD	2005/08/04–present
NSKO	Neskantaga	52.1965	−87.9305	FedNor/GSC-NRD	2005/07/29–present
OTRO	Otter Rapids	50.1818	−81.6286	FedNor/GSC-NRD	2003/06/18–present
PEMO	Pembroke	45.6773	−77.2466	POLARIS	2002/11/13–present
PKLO	Pickle Lake	51.4987	−90.3522	FedNor/GSC-NRD	2004/06/15–present
PLVO	Plevna	45.0396	−77.0753	POLARIS	2004/05/13–present
PNPO	Pukaskwa Provincial Park	48.5956	−86.2846	FedNor/GSC-NRD	2004/06/18–present
RDLO	Red Lake	50.9744	−93.9124	FedNor/GSC-NRD	2004/06/13–2004/09/30
RLKO	Red Lake	51.0704	−93.7585	FedNor/GSC-NRD	2004/11/19–present
RSPO	Restoule Provincial Park	46.0734	−79.7602	POLARIS	2004/08/05–present
SILO	Sutton Inlier	54.4792	−84.9126	FedNor/GSC-NRD	2003/06/09–present
SUNO	Sudbury Onaping	46.6438	−81.3442	FedNor/GSC-NRD	2003/06/23–present
TIMO	Timmins	48.4659	−81.3032	FedNor/GSC-NRD	2005/07/25–present
TOBO	Tobermory	45.2257	−81.5234	POLARIS	2003/07/29–present
VIMO	Victor Mine	52.8173	−83.7449	GSC-NRD	2003/06/11–present
WEMQ	Wemindji, Quebec	53.0535	−77.9737	GSC-NRD	2005/06/23–present
GAC	Glen Almond, Quebec	45.703	−75.478	CNSN	1992–present
KAPO	Kapuskasing	49.450	−82.508	CNSN	1998–present
ULM	Lac du Bonnet, Manitoba	50.250	−95.875	CNSN	1994–present

and solar panels as power sources. The VSAT system enables the stations to transmit data in near-real time to the central data hubs in London (Canada) and Ottawa.

In addition to the POLARIS/FedNor seismograph stations, three CNSN (Canadian National Seismograph Network) broad-band stations were used in the study, providing additional data from southeastern Manitoba, southwestern Quebec and northeastern Ontario.

2 SURFACE WAVE DISPERSION ANALYSIS

A two-station analysis method (after Gomberg *et al.* 1988) was used to investigate fundamental mode Rayleigh wave dispersion across the study region. The use of this method means that the phase effects of the earthquake source function and the common path to the station pair are cancelled out, allowing a regional study even when the major part of the data set consists of far-field teleseismic earthquakes whose paths to Ontario may include both continental and oceanic structures.

The study used data from large (primarily magnitude >5.5) teleseismic or near-teleseismic earthquakes (Fig. 2). Following the selection of appropriate events by magnitude from global bulletins, a further selection criterion based on geometry was applied to the event list. The use of a two-station method in surface wave analysis requires the incoming energy from a given earthquake to lie on or close to the great-circle path between a given pair of seismograph stations. In this case, a 5° tolerance around the ideal great-circle path was used to select the appropriate earthquakes. Following the selection of the events, the data were downloaded from the archives of the Canadian National Seismograph Network, and visually inspected for surface wave quality and coherence. In order to assess the quality of the surface waves fully, the inspection was carried out at a number of different frequency bands within a 30–500 s period range. Only events with a good signal-to-noise ratio and good coherence between both stations of the pair were kept for further analysis. Consideration was also given to potential errors related to wave front propagation; further details are given in the Appendix.

The stations used in this study have a number of different instrument responses, with some stations changing instrumentation partway through their deployment. In order to prevent phase errors from affecting the results of the analysis, it was necessary to ensure that the instrument responses between station pairs were standardized (Darbyshire & Asudeh 2006).

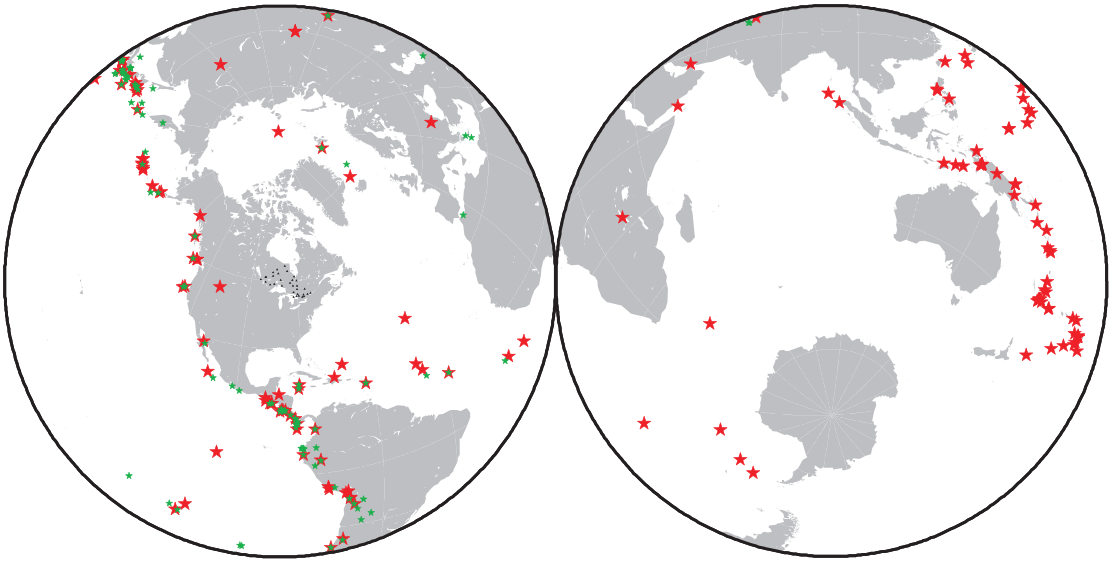

Figure 2. Global distribution of earthquakes used in surface wave analysis (red) and receiver function analysis (green).

The two-station phase velocity dispersion curves were calculated from Rayleigh waves recorded on the vertical component seismograms. We used a modified form of the transfer-function method of Gomberg *et al.* (1988) to perform the calculations. A full description of the method is given in Darbyshire *et al.* (2004); here we give a brief overview.

In the transfer-function method, the seismogram recorded at the station furthest from the earthquake is assumed to be represented by the convolution of the near-station seismogram with an Earth filter whose properties are governed by the crust and mantle structure between the two stations. The phase of the Earth filter is given by $\phi(\omega)$, and is related to surface wave phase velocity as follows:

$$\phi(\omega) = k(\omega)\Delta r = \omega\Delta r/c(\omega), \quad (1)$$

where c is the phase velocity, ω is the angular frequency, k is the wavenumber and Δr is the distance between the stations.

An initial reference dispersion curve (in this case, the CANSD Canadian Shield dispersion curve of Brune & Dorman 1963, with a modification for 40 km thick crust) is used to construct a trial Earth filter. The near seismogram is convolved with the trial Earth filter, and cross-spectral analysis is used to compare the resulting waveform to the far seismogram. The cross-spectrum is used to construct a wavenumber correction term $\delta k\,(\omega)$, and this correction is used to obtain the phase term for the dispersion. At each frequency, the final phase velocity is found by solving the data equations for the wavenumber perturbation, subject to smoothness constraints and weighting factors.

In order to exploit fully the wide bandwidth of coherent teleseismic Rayleigh wave energy, dispersion analysis was carried out at a number of different passbands between ∼30 and 500 s, at which certain frequency ranges were enhanced. In each case, the waveform coherency as a function of period was assessed and the part of the dispersion curve corresponding to highly coherent results was isolated. The sets of results were then combined to produce the final phase velocity dispersion curve. In a few cases, shorter-period passbands were also considered, but there was generally little coherent fundamental-mode signal below ∼20 s period. The use of different passbands in the calculation of the dispersion curves is necessary as the long-period signals are significantly smaller in amplitude than the short-period (∼20–50 s) signals. When the analysis is carried out over the full bandwidth, the relative contribution of the long-period signals is not sufficient to allow a meaningful calculation of the long-period dispersion relation. In addition, the division of the signal into several passbands allows the simultaneous analysis of multiple events that may not have the same signal bandwidth, due to factors such as noise or source characteristics.

The method can be applied both to single earthquakes and to multiple events along the same great-circle path. Initially, each earthquake was analysed separately, and the resulting dispersion curves compared to those from other events in order to remove unstable results, to check whether all events are incident along the same great-circle path and to check for any spurious phase shifts that may result from incorrect application of instrument response corrections. Full simultaneous analysis was then carried out for the different passbands.

In addition to the phase velocity measurements, the method yields error estimates associated with each period. However, these errors represent only statistical estimates which may be attributed to noise contamination, and do not take into account systematic errors or the effects of surface wave multipathing and scattering. They are, therefore, considered to be an underestimate of the true measurement errors. Error bars in the final dispersion curves were generally increased when the results from different passbands were averaged, but these were still considered to under-represent the likely systematic errors. Based on phase velocity error values in previous studies using both real and synthetic data (van Heijst *et al.* 1994, and references therein), new error bars were applied to the data, scaled to increase with increasing period. The size of the new errors ranges from 0.01 km s^{-1} at periods of <30 s to 0.08 km s^{-1} at periods >170 s.

The majority of the two-station paths studied yielded phase velocity curves spanning a period range of ∼25–30 s to ∼150–200 s, though the frequency content of some surface wave arrivals resulted in certain curves having a smaller range, with bias towards the shorter or longer periods for a few paths. The average period range of the dispersion curves allows good constraint of shear wave velocities within the upper mantle to depths of approximately 300 km. Detailed constraint of crustal velocities is not possible, though the average crustal velocity and depth to the Moho will affect the phase velocities at short periods. 133 two-station paths have been

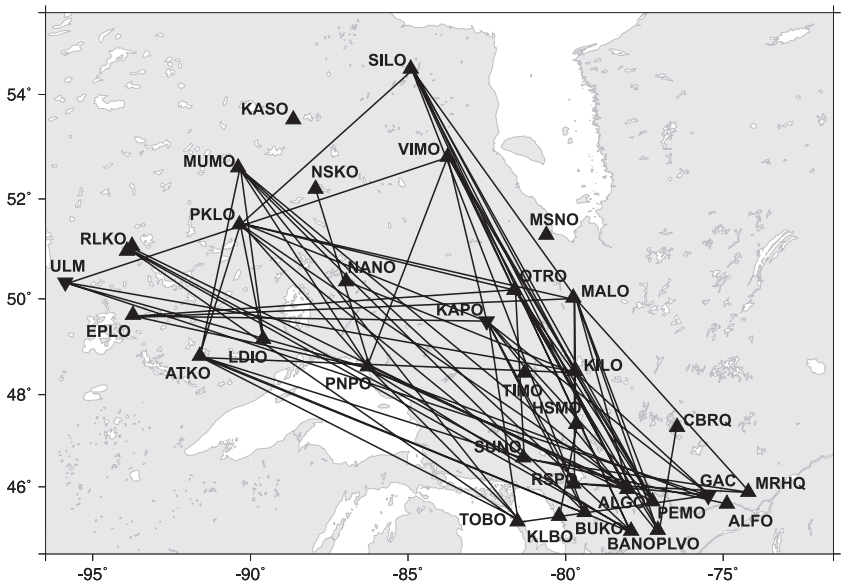

Figure 3. Coverage of stable two-station surface wave paths analysed in this study.

analysed, of which 100 yielded stable, consistent results (Fig. 3). Some stations (e.g. KASO and MSNO; Fig. 1) have yet to be incorporated into the analysis due to their short recording period, but the path coverage across the region is good nevertheless.

A representative sample of the dispersion curves is shown in Fig. 4. Each curve is plotted against two reference curves, CANSD (Brune & Dorman 1963) and a dispersion curve calculated from the iasp91 global reference model of Kennett & Engdahl (1991). CANSD provides a useful reference for the region, as it represents an average dispersion characteristic for the Canadian Shield as a whole. The curves exhibit characteristics typical of continental shields, with phase velocities generally close to, or above, those of CANSD. However, within this range, there is significant variation between the individual dispersion curves. Of particular interest are two properties: the absolute phase velocities and the curvature of the phase velocity data with respect to period. The latter property is an important qualitative tool in the determination of lithospheric thickness variations. Assuming the presence of a 'lid' of high-velocity upper-mantle material representing the seismological lithosphere, the character and approximate depth of the base of the lid can be inferred by inspecting the period range at which the gradient of increasing phase velocity flattens out. In more extreme cases, where a significant low-velocity zone exists beneath the lithospheric lid, the phase velocities may even decrease slightly at intermediate periods.

The nine curves shown in Fig. 4 are arranged approximately according to the geographic region they sample, with the western Superior on the left, the central regions in the middle and eastern Ontario on the right. The northernmost path of each set appears at the top, and the southernmost path at the bottom. Within this subset of dispersion curves, a large range of properties are apparent. In eastern Ontario, phase velocities at intermediate periods increase to the north–northeast, with velocities significantly higher than CANSD for the MALO-SILO path. The period at which the curve flattens out or decreases slightly in velocity also increases to the north, suggesting a thickening of the lithospheric lid. Most of the central Superior paths show phase velocities similar to those of CANSD, though the changes in curvature suggest that the lithospheric thickness also changes across this region. In the southernmost part of the region, however, where paths cross Lake Superior, the phase velocities lie slightly below CANSD, indicating an anomalous velocity structure compared to paths further to the north. In the western Superior, the pattern of phase velocity variation again lies close to CANSD for NW–SE and WNW–ESE paths. However, for paths sampling a WSW–ENE direction, such as ULM-VIMO, the phase velocities are significantly different. In this case, while the curvature with respect to period is fairly similar to that of many other paths, the absolute phase velocities are greatly elevated. The anomalously fast paths cross over several paths for which the phase velocities are relatively close to CANSD, so an unusually fast mantle shear wave velocity somewhere along the path is an unlikely explanation for the phase velocity curves. However, the orientation of the anomalous paths matches well with the fast direction of *SKS* splitting measured in the Western Superior (e.g. Silver *et al.* 1993; Kay *et al.* 1999a; Frederiksen *et al.* 2006b), suggesting that the most likely explanation for the high phase velocities is strong anisotropy in the lithosphere.

3 MODELLING OF SHEAR WAVE VELOCITY STRUCTURE

30 individual two-station paths or composites of geographically close two-station paths were selected for further analysis, to determine shear wave velocity structure beneath northern and eastern Ontario. Selection of the paths was based on geographical location (we wished to analyse a representative set of paths for different areas of northern and eastern Ontario), path length, and the range of periods at which the phase velocity was measured successfully. In regions of eastern Ontario where several two-station paths are close together, some of the individual results were averaged to produce a composite curve for analysis. Following the method of Shapiro *et al.* (1997), we used a two-stage process to calculate 1-D velocity-depth models representing the average crust and upper-mantle structure along each two-station path.

3.1 Linearized inversion and model simplification

Initially, a linearized inversion technique was used to determine the best-fitting velocity-depth model for each dispersion curve. Two

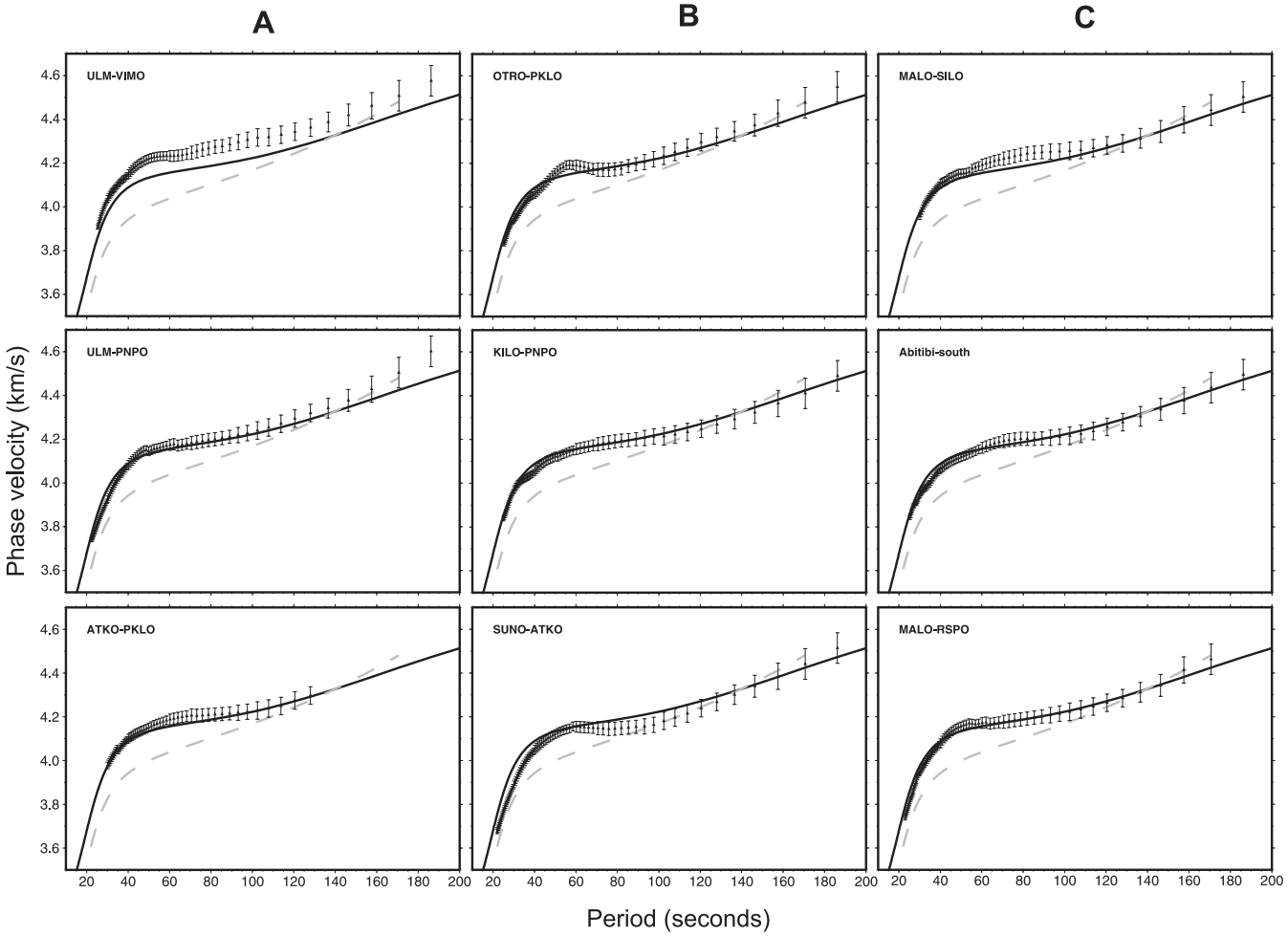

Figure 4. Examples of dispersion curves calculated using the two-station method, grouped according to region. (A) Western Superior, (B) Central Superior (C) Eastern Ontario Superior/Grenville. For curves derived from composite two-station paths: 'Abitibi': OTRO, KILO, KAPO; 'south': ALGO, BANO, BUKO, PEMO, PLVO; 'north': SILO, VIMO; 'east': GAC, ALFO, MRHQ. The lines shown on the figure are synthetic dispersion curves calculated from significant representative velocity models. Solid line: 'CANSD' model (Brune & Dorman 1963); dashed line: iasp91 global reference model (Kennett & Engdahl 1991). The curves are plotted with the error bars used in the velocity modelling scheme.

different methods were tested, and the smoothest result was chosen. The first method was the damped least-squares inversion scheme *surf 96* of Herrmann & Ammon (2002), in which the velocity model is parametrized as a stack of relatively thin layers (5–15 km in the crust and 10–20 km in the mantle). The models were parametrized to a depth of 600 km, well below the maximum depth range at which the shear wave velocity is directly constrained by the fundamental-mode Rayleigh waves, but taking into account the fact that the velocity increase into the transition zone has some effect on the longest-period phase velocities. The second method used was that of Maupin & Cara (1992), in which the parametrization of the model is expressed in terms of velocity gradients and a depth-wise correlation constraint is applied to smooth the models. The initial model used was based on the iasp91 model of Kennett & Engdahl (1991), but using a 40 km thick crust and a higher velocity in the uppermost mantle. Following the estimates of upper-mantle shear wave velocity given by Rondenay *et al.* (2000a), the initial model has a constant upper-mantle velocity of 4.6 km s^{-1} to a depth of 280 km (at which depth the iasp91 shear wave velocity exceeds 4.6 km s^{-1} for the first time), then follows the iasp91 velocities to the base of the model.

The resulting velocity models were first checked for consistency between the two inversion methods, then the major features of each velocity-depth profile were identified. Each model was then simplified to seven or eight layers, from the surface to 500 km depth. Table 3 indicates the parameters used in the simple models. The seven- or eight-layered models were then used as the input to a Monte-Carlo modelling scheme.

3.2 Monte-Carlo modelling

In the modelling scheme of Shapiro *et al.* (1997), a simple layered model is used as input, taken from the best-fit model obtained from linearized inversion. Both the shear wave velocity of a given layer and the interface depths between layers are perturbed randomly, within limits set by the user, and subject to constraints (Table 3). A synthetic dispersion curve is calculated and the match of the synthetic curve to the dispersion data is calculated using a misfit function. The user chooses a confidence limit for the misfit, such that the resulting synthetic dispersion curves lie within the data error bars (see Fig. 6). If the misfit function falls within the confidence limit, the model is accepted and used as the basis for a new perturbation; otherwise it is rejected and the previous accepted model is given a new perturbation for further testing. In this way, tens of thousands of

Table 3. Layer parameters and constraints for Monte-Carlo modelling (Shapiro *et al.* 1997). The layer marked '∗' is only used if a 7-layered model cannot provide an acceptable match to the dispersion data.

Layer number/interface	Description	Constraints used in modelling
0	Upper crust	$3.3 \leq$ Vs ≤ 3.8 km s^{-1}
1	Lower crust	$3.8 \leq$ Vs ≤ 4.2 km s^{-1}
	Moho	$35 \leq$ depth ≤ 45 km
2	Top mantle	Vs ≤ 4.9 km s^{-1} ∗
3	Mantle lithosphere	Vs ≤ 4.9 km s^{-1}, thickness ≥ 50 km
4	Asthenosphere	Vs ≤ 4.9 km s^{-1}, thickness ≥ 50 km
5	Deep upper mantle	Vs ≤ 4.9 km s^{-1}, thickness ≥ 50 km
	410 km discontinuity	$400 \leq$ depth ≤ 420 km
6	Transition zone 1	iasp91 Vs for 440 km, ± 0.02 km s^{-1}
7	Transition zone 2	iasp91 Vs for 480 km, ± 0.02 km s^{-1}

models are tested, so that a large parameter space may be explored, and the possibility of the solution being trapped in a secondary minimum is avoided.

The perturbations applied in the modelling process were 0.2 km s^{-1} in shear wave velocity and 2–20 km in interface depth, with the allowable depth perturbation increasing with successive deepening layers. The subtransition-zone layers were fixed in velocity and depth to within a small range around the iasp91 values, since there is little direct constraint on shear wave velocity at these depths. Moho depths were constrained to lie within a range of 35–45 km, typical for the region as a whole (e.g. Perry *et al.* 2002), and further conditions were applied to constrain mantle properties to physically realistic limits.

A three-step process was used in the random search, in order to start with a large parameter space but to jump quickly to the optimal part of the model space before beginning a detailed localized search. The program was initially run 500 times with a large confidence limit. At the end of this initial run, the program jumped to the best-fitting model of the set and used it as the basis for a second run of 500 models with a smaller confidence limit. The best-fitting model from the second set was then used as the basis for the final search, in which a small confidence limit was imposed in order to limit the spread of the solutions around the dispersion data. In addition, multiple modelling runs were carried out for each dispersion curve, using a different 'seed' number to begin the random perturbation process each time. In this way, the effect of any bias in the results due to the random number generator was removed.

Each modelling run generated 50 000–100 000 models, of which ∼1000 solutions were accepted. From these 1000 solutions, a mean mantle model was calculated. As the mean value is calculated for a large number of different depths, the resulting model has a velocity gradient as opposed to a simple seven- or eight-layered structure, and thus likely better represents the velocity–depth profile for each interstation path.

4 SHEAR WAVE VELOCITY STRUCTURE ACROSS NORTHERN AND EASTERN ONTARIO

Representative shear wave velocity models for the two-station paths across the study region are shown in Figs 5–9. Each figure shows the isotropic 1-D structure to a depth of 350 km, beneath which there is very little direct constraint from the dispersion curve data. The structure below 400 km depth is constrained in the modelling procedure to be close to the iasp91 velocity profile (shown in the figures as a dashed line). In each case, the ∼1000 layered velocity models from each of 3 or 4 runs of the Monte-Carlo procedure are shown as pale lines, and the resulting average models are shown as heavy solid lines. The amount of variation in isotropic mantle velocity structure across the region is immediately apparent; while all models show a high-velocity lid structure in the upper mantle, the depth extent of the lid and the average velocity within it differs significantly. In some cases, the base of the lid is relatively well defined by the models, but in others the lid velocity decreases very gradually or stays relatively constant with increasing depth. The nature of the mantle beneath the lid is also variable; for certain paths the velocity does not drop significantly below iasp91 but, in many cases, a significant low-velocity zone is apparent.

In our description of the models, we divide the study area into five partially overlapping regions:

(i) Western Superior: samples paths between ∼95°W and ∼85°W.

(ii) Central Superior: samples paths between ∼90°W and ∼79°W.

(iii) Northeast: samples paths between ∼48.5°N and 55°N, 85°W and 79°W.

(iv) East: samples paths between ∼45°N and 50°N, 82°W and 74°W.

(v) Southeast: samples the far southeast of the study area (45–47°N, 82–74°W).

4.1 Defining the lithosphere and its base

The cratonic lithospheric mantle, in seismological terms, is generally considered to be represented as a 'lid' of elevated velocities with respect to global reference models. The elevated velocities typically extend to 150–300 km depth (e.g. Debayle & Kennett 2000; Gung *et al.* 2003; van der Lee & Frederiksen 2005). Defining the base of the lithosphere, however, proves to be a more difficult issue, especially in cases such as surface wave studies, where there is little sensitivity to boundaries and interfaces, and a gradient model can match the data equally well as the more artificial layered models. Attempts have been made by many authors carrying out surface wave studies to characterize the base of the lithosphere. The nature of the negative velocity gradient in the bottom section of the high-velocity lid is invoked by some (e.g. Cotte *et al.* 2000; Priestley & Debayle 2003), whereas others use the velocity perturbation with respect to a global reference model such as iasp91 as a guide, defining the base of the lithosphere to be the depth at which the velocity drops to within 1.5–2 per cent of iasp91 (e.g. Gung *et al.* 2003). In this study, we see that the nature of the negative velocity gradients

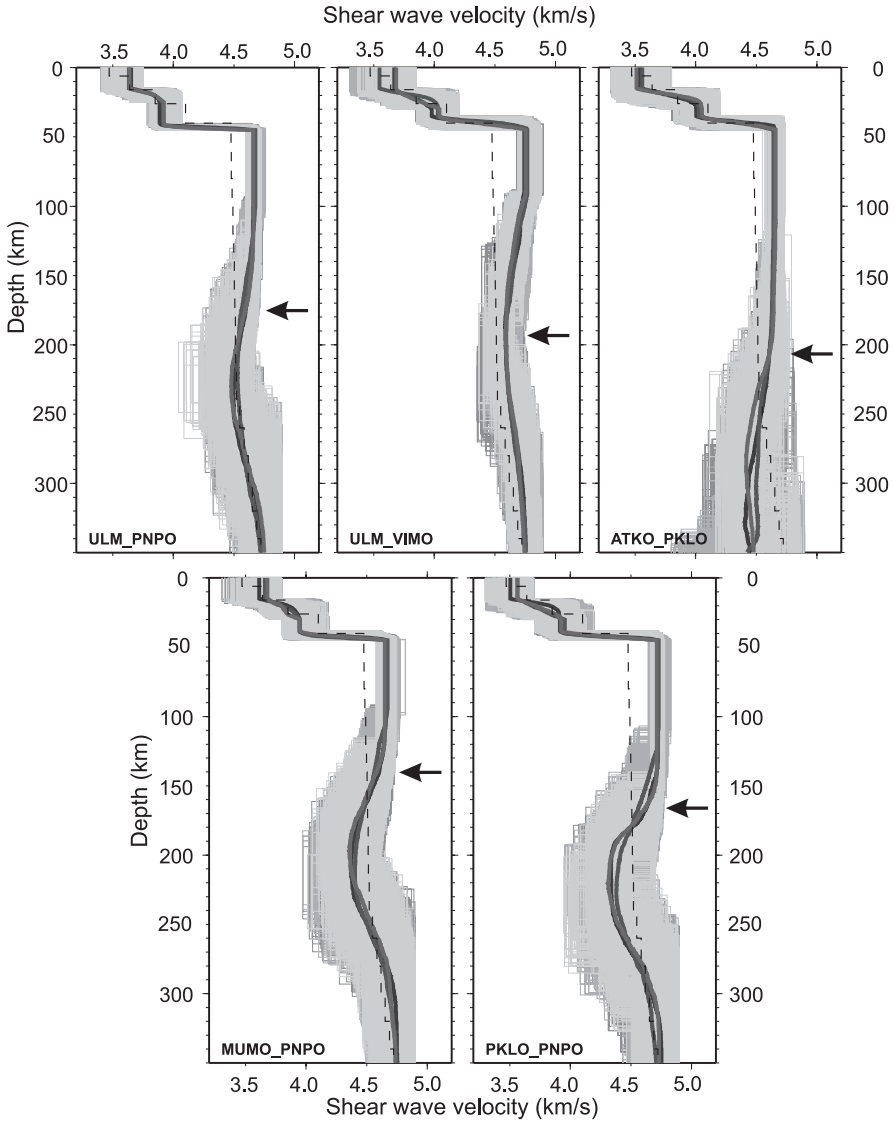

Figure 5. Examples of velocity models calculated using the Monte-Carlo method of Shapiro *et al.* (1997). Dashed line: global reference velocity model iasp91. The pale grey lines show individual layered models that provide an acceptable match to the data; different shades represent the results from different model runs. The thicker solid lines show the average results from each of the 3 or 4 modelling runs carried out. An arrow marks the depth at which the velocity in the lithospheric lid decreases to within 1.7 per cent of iasp91 mantle velocities, inferred to represent the base of the seismological lithosphere. The two-station path is labelled at the bottom left of each profile. This set of paths samples the western Superior region.

at the base of the lithospheric lid varies greatly, and therefore, we choose to work with the latter definition of lithospheric thickness. We take a middle value of 1.7 per cent within the commonly used 1.5–2 per cent range for the perturbation from iasp91 that represents the base of the lithosphere. The value may be regarded as somewhat arbitrary, but it allows us to make direct comparisons of lithospheric thickness across northern and eastern Ontario. It is appropriate for us to attempt to constrain this parameter across northern Ontario given the strong interest in lithospheric thickness estimates; for example, from the field of diamond exploration.

We inspected the individual results from the Monte-Carlo modelling scheme to assess whether models consisting of a high-velocity 'lid' overlying a low-velocity zone are required by the data. For the majority of paths, >95 per cent of all successful models require a low-velocity zone, though both the velocity contrast between the 'lid' and low-velocity zone, and the velocity-gradient vary from path to path. For a few paths, a lower proportion of models require a low-velocity zone to match the data; in these cases, the base of the lithosphere cannot easily be defined. We also considered the average depth at which the base of the high-velocity lid occurred. In the case of paths for which the transition zone between the 'lid' and low-velocity zone was well defined, the average depth to the lid base lay within ∼30 km of the lithospheric thickness defined by the 1.7 per cent contour above δV_s.

4.2 Western Superior

Fig. 5 shows the velocity models for Western Superior paths, with the exception of path ULM-VIMO, which spans most of the westeast section of the study region. The region is characterized by velocity models with a well-developed lithospheric lid of ∼150–180 km thickness, and a definite low-velocity zone beneath the lid. This zone is strongest towards the easternmost paths (MUMO-PNPO

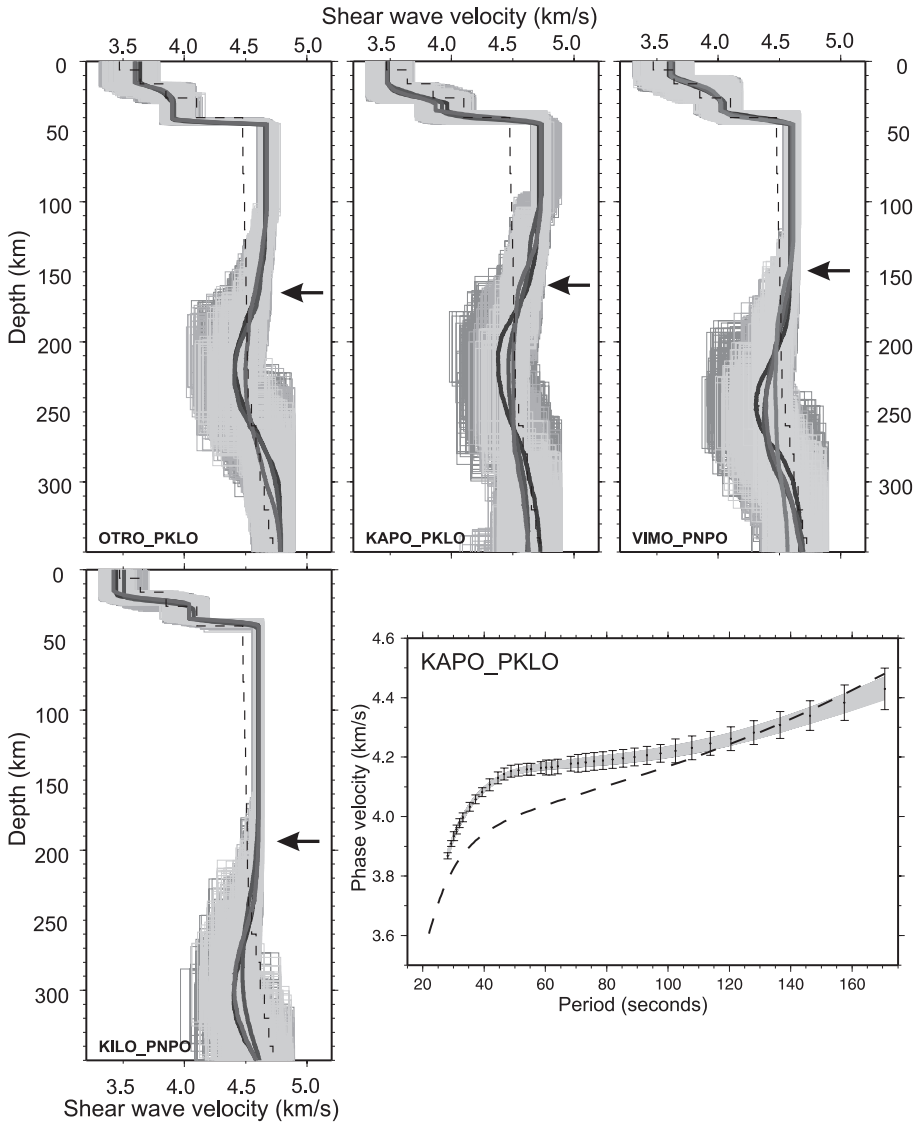

Figure 6. Models for the central Superior region. See Fig. 5 for plotting conventions. Also shown is the dispersion data (points with error bars) and corresponding synthetic dispersion curves (grey lines) for path KAPO-PKLO. The dashed line corresponds to the iasp91 global reference model.

and PKLO-PNPO), for which the shear wave velocities drop below iasp91 in the mid-upper mantle. For path ATKO-PKLO, the models suggest a thicker lithospheric lid; however, the period range of the dispersion data for this path (up to 130 s as opposed to the more typical 170–200 s; see Fig. 4) is such that constraint is likely to be poor below ∼200 km depth. For path ULM-VIMO, the high phase velocities translate to high shear wave velocities (>6 per cent above iasp91) in the upper section of the lithospheric lid and a gradual decrease in velocity between 90 and 180 km depth. The continuing high velocities mean that the thickness of the lithosphere as defined by the 1.7 per cent velocity anomaly exceeds 200 km. It should be noted in this case that the high apparent lid velocities are likely to arise from the isotropic modelling of a path that samples the fastest wave velocities in an anisotropic region.

4.3 Central Superior

The region defined here as 'central Superior' encompasses a relatively wide range in geographical extent and path orientation, giving rise to significant variability in the velocity models (Fig. 6). The nearby paths OTRO-PKLO and KAPO-PKLO both exhibit similar characteristics to the western Superior models, with a well-developed lithospheric lid of velocity ∼5 per cent above iasp91 and thickness ∼160–180 km. The low-velocity zone at ∼190–250 km depth drops slightly below the iasp91 model. In contrast, paths KILO-PNPO and VIMO-PNPO have lower velocities in the lithospheric lid (2–3 per cent above iasp91) and different lithospheric thicknesses; ∼190 and 150 km, respectively. The low-velocity zone in the ∼210–300 km depth range for VIMO-PNPO is relatively well-defined; however the low-velocity zone for path KILO-PNPO lies in the depth range at which the direct constraint on shear wave velocity from the dispersion curve deteriorates.

4.4 Northeast

In this region, the velocity models (Fig. 7) 'Abitibi-north' (a composite of paths from stations KAPO, KILO and OTRO in the south to VIMO and SILO in the north) and MALO-SILO show the thickest

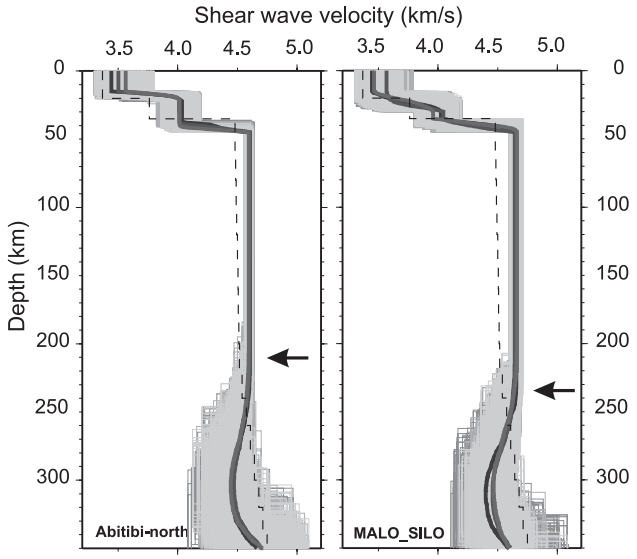

Figure 7. Models for northeast Ontario. See Fig. 5 for plotting conventions.

lithospheric lid of the entire study region (210–240 km). Lithospheric velocities are of average values (close to 3 per cent above iasp91) for the Abitibi-north path, but higher (close to 4 per cent) for path MALO-SILO. Since MALO-SILO lies at the far edge of the path coverage, it is not clear whether this velocity difference is attributable to anisotropy or to the effect of higher-velocity structure further to the northeast. In both cases, there is an indication of a low-velocity zone beneath the lithospheric lid, but the range of acceptable models shown, and the fact that the depths are close to the resolution limit of the dispersion data, means that this feature should not be considered robust.

4.5 East

The eastern Ontario Superior appears, from the nature of the velocity models calculated for the region, to be the most complex part of the study area. The model characteristics, the thickness of the lithosphere and the velocity anomalies vary significantly depending on both geographical position and path orientation, suggesting that the region may be highly anisotropic in nature. For the paths modelled, the apparent lithospheric thickness varies from ∼100 km

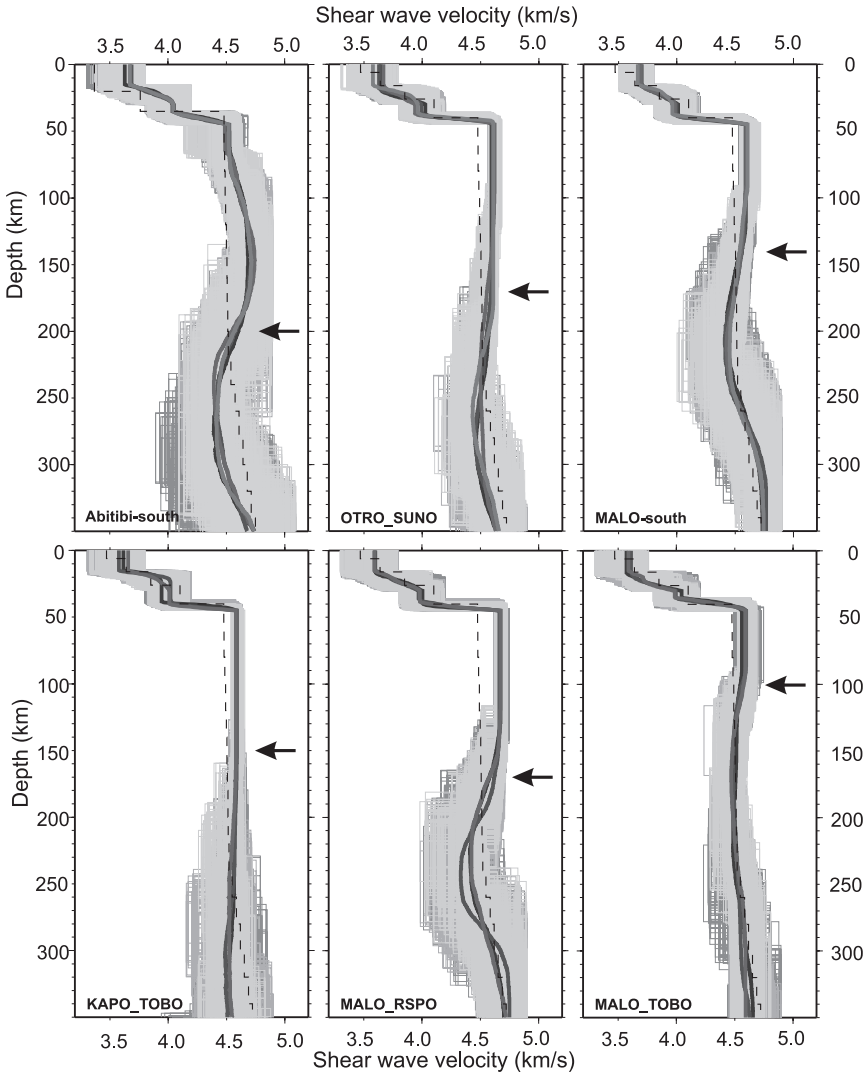

Figure 8. Models for eastern Ontario. See Fig. 5 for plotting conventions.

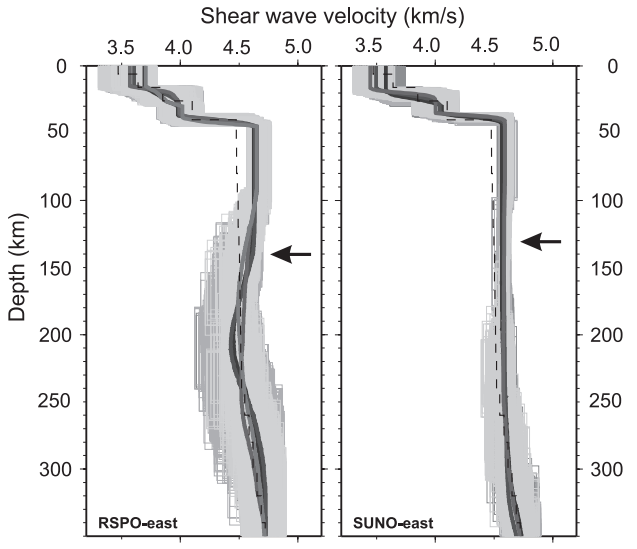

Figure 9. Models for southeast Ontario. See Fig. 5 for plotting conventions.

to ∼220 km, and the velocity perturbation with respect to iasp91 varies from 2–3 to 4–5 per cent in the lithospheric lid. Of the six paths whose velocity models are shown in Fig. 8, three (MALO-south, OTRO-SUNO and MALO-RSPO) show similar characteristics to models from the western and central Superior, with a simple but distinct lithospheric lid and low-velocity zone. In contrast, path KAPO-TOBO is modelled with near-constant velocity beneath the Moho, with velocities higher than iasp91 down to ∼240 km depth (though the lithospheric thickness defined by the 1.7 per cent dV_S limit is ∼150 km). Beneath this depth, the models indicate velocities significantly lower than iasp91, though the resolution is relatively poor in this depth range. The average mantle model for path MALO-TOBO shows a lithospheric lid of thickness ∼110 km, beneath which the shear wave velocities lie close to iasp91. However, the velocity anomaly within the lid is relatively small (∼2–3 per cent above iasp91) and some models show uppermost mantle velocities very close to iasp91. The most unusual velocity models are those that are derived from NNW–SSE paths between the 'Abitibi' stations KAPO, KILO and OTRO and the 'south' stations ALGO, BANO, PEMO and PLVO. A composite result, 'Abitibi-south', is shown here. In this case, a simple 7-layered model was insufficient to match the dispersion data to an acceptable degree. Use of an 8-layered model resulted in an adequate match, but the model shows a more extreme velocity variation in the upper-mantle section than most other paths in the study. The average model has an uppermost mantle layer with velocities <2 per cent higher than iasp91, below which lies a high-velocity lid between ∼90 and ∼210 km depth, in which the average velocity is ∼4–5 per cent above iasp91. Beneath the lid, the ∼220–300 km depth range is characterized by a strong low-velocity zone, in which the average model has a minimum velocity of ∼4.2–4.3 km s^{-1}. The synthetic dispersion curves lie within the data error bars, but they do not fully match the curvature of the data, suggesting that a more extreme variation in the apparent mantle structure may be needed. If this is the case, then it is most likely that a 1-D isotropic velocity model along these paths is too simple to model the average structure.

4.6 Southeast

The two velocity-depth models that provide constraint on eastwest paths through southeast Ontario are surprisingly different in character (Fig. 9). Path RSPO-east has a well-developed 'shield-type' structure with a high-velocity lid of thickness ∼150 km overlying a low-velocity zone in the 170–240 km depth range. In contrast, the velocity model for the neighbouring path SUNO-east shows only a hint of a lithospheric lid; instead, the average velocity stays relatively constant from the Moho to at least 200 km depth, then rises gradually. The maximum upper-mantle velocity is 2–3 per cent above iasp91, dropping to 1.7 per cent at ∼130 km depth. The two paths are close in terms of both location and angle of orientation, so it is not obvious why the two velocity models are so different. One possible explanation may be structural differences in the region between RSPO and SUNO, but these remain unresolved.

5 CRUSTAL THICKNESS VARIATIONS: RECEIVER FUNCTION ANALYSIS

Although published crustal thickness measurements are available at several locations across the Superior craton, mainly from large-scale refraction experiments (Perry *et al.* 2002, and references therein), the coverage is too sparse for mapping Moho depth trends throughout the study region. Thus, in order to determine if variations in lithospheric structure are also reflected in crustal-thickness trends, we have used a modified version of the stacking technique of Zhu & Kanamori (2000) to estimate Moho depth. Their method provides efficient and robust 'point' estimates of Moho depth and Vp/Vs, by exploiting crustal reverberations that occur within the coda of teleseismic *P* phases. By stacking several modes of crustal reverberations, this technique is rendered largely insensitive to uncertainties in crustal velocity. The technique is described in detail by Eaton *et al.* (2006) and briefly summarized below.

Receiver functions are a well-established tool for imaging structure of the crust and upper mantle beneath a seismograph station (Langston 1977; Owens *et al.* 1984; Bostock & Cassidy 1995). They are comprised of waveforms caused by *S*-wave scattering from interfaces in the lithosphere, particularly the Moho. Prominent among these signals are the *Ps* Moho converted phase, as well as *PpPs*, *PsPs* and *PpSs* crustal reverberations (Fig. 10). In principle, the three unique arrival times of these phases (*tPs*, *tPpPs* and *tPsPs* + *PpSs*) can be used to form a non-linear system of equations for three unknown quantities: crustal thickness (H), Vp and Vs (Zandt *et al.* 1995; Zandt & Ammon 1995). In practice, these arrival times are relatively insensitive to *P*-wave velocity (Zhu & Kanamori 2000). It is therefore, common to use an assumed value for Vp and solve for H and the ratio Vp/Vs.

Zhu & Kanamori (2000) have developed an efficient, semi-automated technique to estimate H and Vp/Vs, by a simple weighted summation of *Ps*, *PpPs*, *PsPs* and *PpSs* signals for a selected set of teleseisms. As illustrated in Fig. 10, the summation is performed for a wide range of trial values of H and Vp/Vs, and the largest stacked value is selected to obtain the best parameters. This method has the advantage that it eliminates the need to pick arrival times for each phase. Eaton *et al.* (2006) have modified this method slightly by introducing a semblance filtering technique to reduce noise, and using standard error as a measure for parameter uncertainties. These modifications to the algorithm of Zhu & Kanamori (2000) provide reduced uncertainties in H and Vp/Vs. As noted by Eaton *et al.* (2006), parameter trade-offs are also captured in a more natural way, since uncertainties derived from curvature of the error surface (e.g. Zhu & Kanamori 2000) generally do not decrease as more events are considered. In contrast, the standard error generally decreases with the inclusion of more data. This behaviour of uncertainty is in

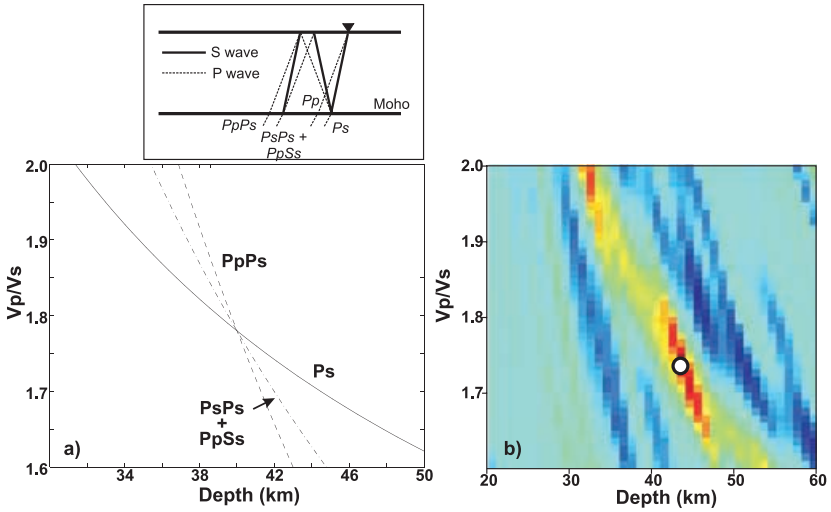

Figure 10. Receiver function stacking method of Eaton (2006) applied to station PNPO. (a) Ray diagram for converted and reverberative phases in a single-layered model and kinematics of the *PpPs*, *PsPs*, *PpSs* and *Ps* phases versus *Vp*/*Vs* ratio and crustal thickness. The intersection point of the curves coincides with the values appropriate to the station. (b) Semblance-weighted stack values for all high-quality events. The red region signifies the highest stack values and the white circle indicates the optimum crustal thickness and *Vp*/*Vs* ratio obtained from the stack.

Table 4. Moho depth (*H*) and *Vp*/*Vs* ratios for stations for which receiver function analysis was carried out.

Station	*H* (km)	Error in *H* (km)	*Vp*/*Vs*	Error in *Vp*/*Vs*
ATKO	44	0.46	1.71	0.011
EPLO	41	0.45	1.73	0.015
HSMO	32	0.83	1.76	0.038
KAPO	48	0.62	1.71	0.020
KILO	35	0.45	1.87	0.012
LDIO	41	0.49	1.82	0.021
MALO	37	0.36	1.77	0.024
MUMO	38	0.31	1.74	0.015
NANO	42	0.67	1.75	0.022
OTRO	41	0.81	1.79	0.029
PKLO	37	0.35	1.81	0.012
PNPO	44	0.54	1.69	0.017
RDLO/RLKO	42	0.32	1.77	0.011
RSPO	34	0.40	1.80	0.015
SILO	38	0.29	1.73	0.011
SUNO	34	0.39	1.79	0.018
VIMO	44	0.66	1.73	0.010
WEMQ	39	0.38	1.72	0.014

accordance with the concept that the result is more certain when more data are used.

This method for determining crustal thickness has been applied to 18 stations, based on M > 6 teleseismic events during 2003–2006. A listing of the events used for this analysis is provided as supplementary data (see the online version of the article); the results of the analysis are given in Table 4 and shown in Fig. 11. Uncertainties given in Table 4 represent 95 per cent confidence limits derived from standard error contours around the maximum value using the semblance-weighted stacking technique of Eaton *et al.* (2006). We remark that the derived crustal thickness and *Vp*/*Vs* values should be regarded as apparent values, since this stacking technique treats the crust as a single homogeneous layer. Beneath the western and central Superior, the apparent crustal thickness ranges from 32 to 48 km, with a general trend towards thicker crust in the south than the north.

Although the uncertainties in apparent *Vp*/*Vs* values are considerably greater than for crustal thickness, the inferred *Vp*/*Vs* distribution shows consistent trends. Relatively high values (1.80–1.82) characterize some areas adjacent to the Great Lakes (stations PLKO, LDIO, RSPO) and within the Abitibi Greenstone Belt (KILO), whereas lower values of 1.69–1.75 are found for most other areas of the Superior. The highest values of apparent *Vp*/*Vs* are associated with stations within the region influenced by the Keweenawan (1.11–1.09 Ga) Mid-continent Rift event, where voluminous mafic magmatism has altered the bulk crustal composition (Thurston *et al.* 1991), or within the Abitibi Greenstone Belt where mafic rock units are common. Compiled measurements of *Vp*/*Vs* from representative crustal rocks (Holbrook *et al.* 1992) show mean values of 1.86 and 1.72 for *Vp*/*Vs* of gabbro and granite, respectively. Thus, despite large uncertainties, the apparent *Vp*/*Vs* results are generally consistent with expectations of bulk crustal composition based on regional geological considerations.

The Moho depths modelled by the receiver function analysis in northern Ontario are broadly similar to the results from Lithoprobe reflection/refraction profiles conducted in the Abitibi, Kapuskasing Structural Zone and western Superior regions (Ludden & Hynes 2000; Percival & West 1994; Musacchio *et al.* 2004, respectively). The changes in *Vp*/*Vs* ratio from south to north along ∼90°W are consistent with the inference of high-velocity mafic material beneath the southern section of the western Superior northsouth line (*cf.* Kay *et al.* 1999b; Musacchio *et al.* 2004), though the *Vp*/*Vs* ratio is considerably lower to the east and west. A high-density feature is also modelled at depth in a similar region by 3-D Bouguer gravity inversion (Nitescu *et al.* 2006).

6 DISCUSSION

6.1 Variations in mantle structure

A summary of information on lithospheric thickness and average velocity anomaly in the lithospheric lid is presented in Fig. 12. The two-station paths for which the 1-D average shear wave velocity structure was modelled in this study are plotted, and colour-coded

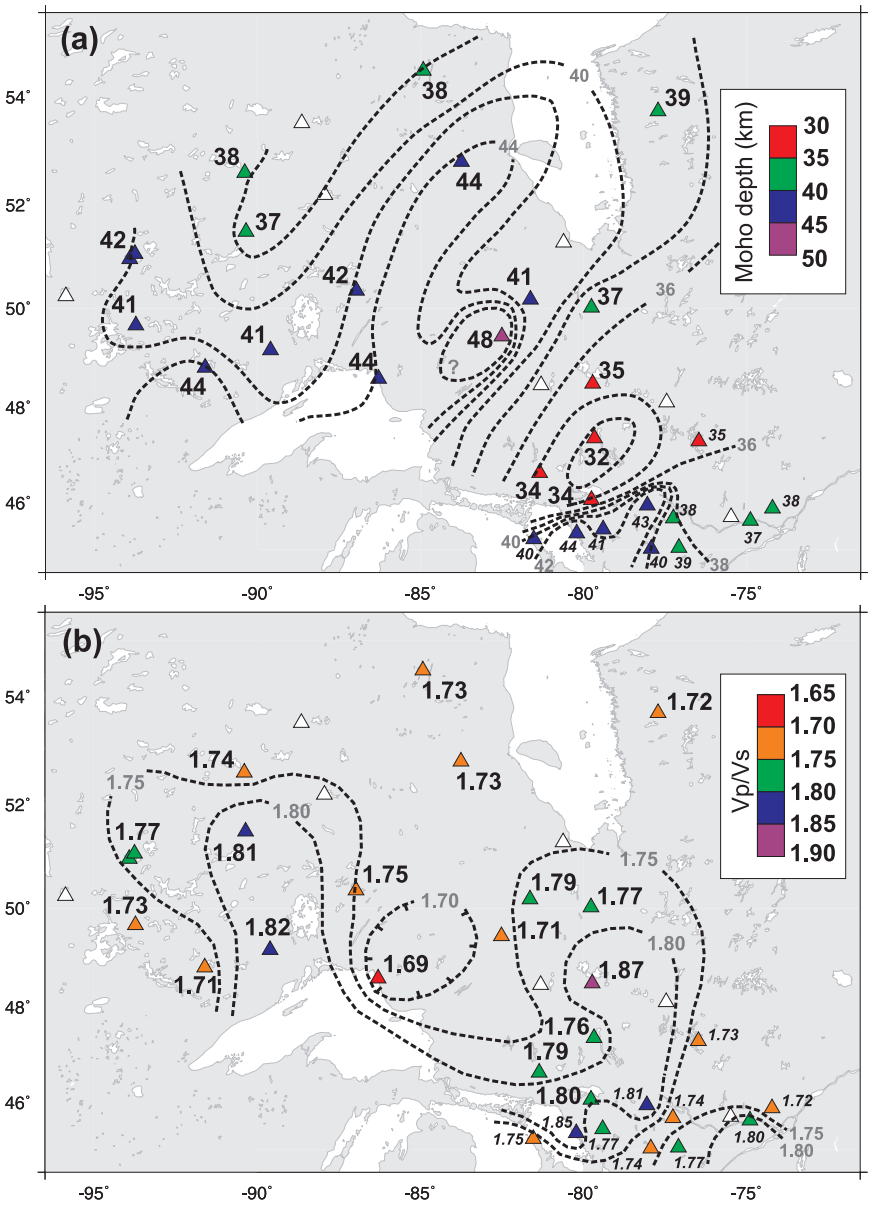

Figure 11. (a) Crustal thickness and (b) *Vp/Vs* measurements for northern Ontario derived from receiver function analysis. Station location markers (triangles) are colour-coded according to results. White triangles denote stations for which no analysis was carried out. Measurements given in large non-italic font are those made for FedNor and CNSN stations in this study; italic font gives measurements made by Eaton (2006).

according to the lithospheric properties inferred from the modelling process. The map of lithospheric thickness is further characterized (by line style) according to the level of definition of the base of the lithosphere. The classification results from a combination of visual inspection of the models and quantitative assessment of the presence and depth of low-velocity zones beneath the lithospheric lid.

In terms of both lithospheric thickness and velocity anomaly, it is difficult to characterize a regional-scale pattern in the results in any detail. The results appear to depend strongly on path length (longer paths may sample a number of different geological subprovinces of the Superior and Grenville, for example) and on path orientation, the latter factor suggesting that anisotropy plays an important part in the understanding of regional structure. This is illustrated in Fig. 13 for paths sampling the Western Superior Province and eastern Ontario (using the geographic definitions given in Section 4). In qualitative terms, it is possible to divide the study region into three broad categories:

(i) Northeastern Ontario (∼48°N to 55°N, 85°W to 79°W) is characterized by the thickest lithosphere, ranging from ∼200 to 240 km along the paths modelled. Simple structures are sufficient to match the data. Although the average models show a low-velocity zone at depths of >250 km, the resolution of the data is insufficient to resolve this as a robust feature.

(ii) The western and central Superior paths (∼48°N–54°N, 95°W–80°W) are generally best modelled by a lithospheric thickness of ∼140–180 km. The velocity-depth profiles show a strongly developed high-velocity lithospheric lid, generally underlain by a moderate low-velocity zone. However, paths aligned with a WSW–ENE direction exhibit high phase velocities and hence high

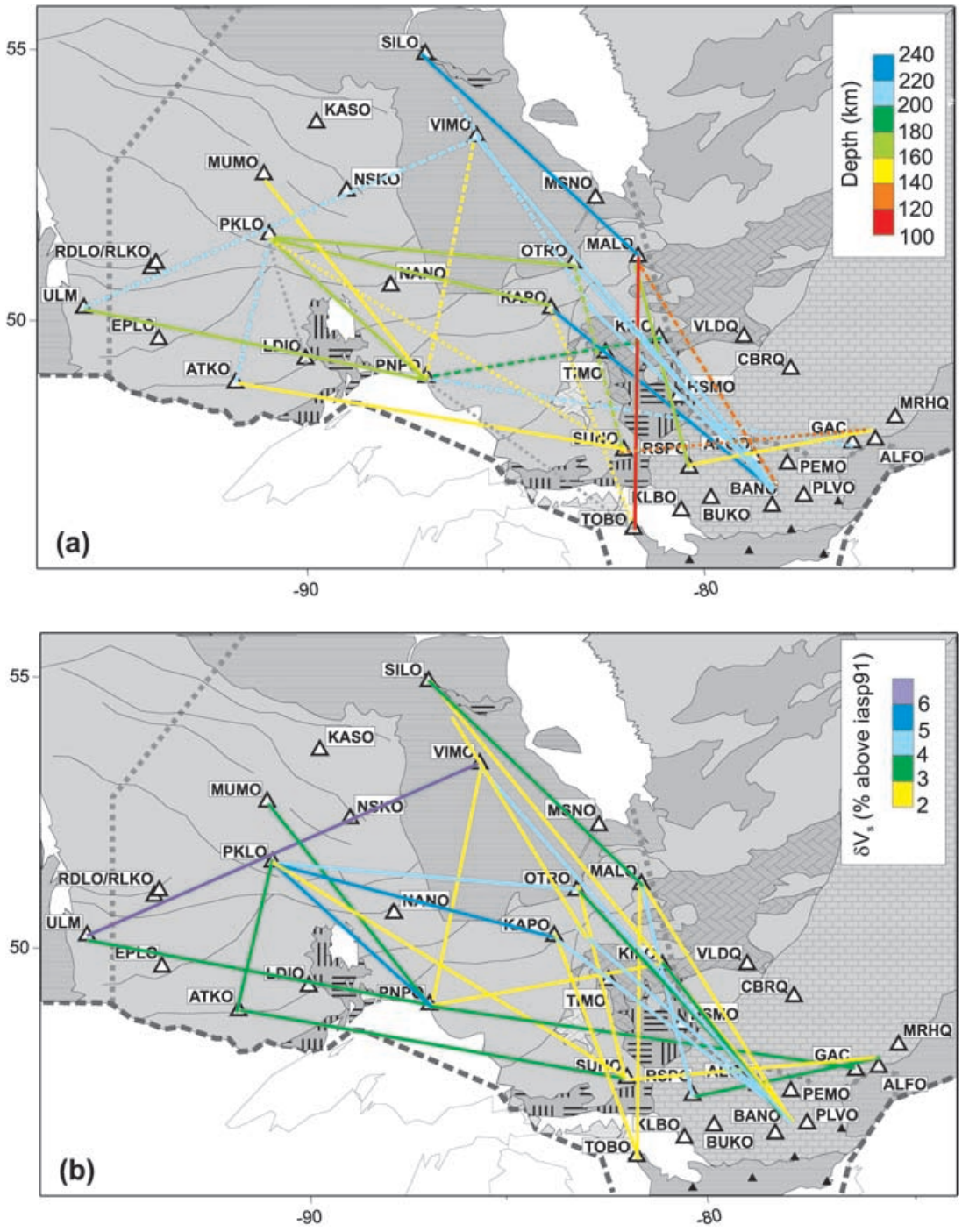

Figure 12. (a) Map of lithospheric thickness along the modelled two-station paths, defined by the depth at which the velocity in the lithospheric lid decreases to within 1.7 per cent of the iasp91 reference model. Grey lines denote paths for which the lid velocity remained within 1.7 per cent of iasp91. Solid lines indicate that the base of the lithosphere is well defined by strong negative velocity-gradients at its base. Dashed lines indicate a more gradual transition to the sublithospheric low-velocity zone, and dotted lines indicate models for which the base of the lithosphere is undefined by negative velocity-gradients. (b) Average per cent velocity perturbation above iasp91 in the lithospheric lid.

apparent lithospheric velocities compared to the other paths crossing the region.

(iii) Eastern Ontario (∼45°N–50°N, 82°W–74°W) exhibits the largest variation in mantle properties compared to the extent of the geographical area, with apparent lithospheric thickness varying from ∼100 km to almost 220 km, and a similarly variable apparent lithospheric velocity. The thickest and fastest lithosphere is modelled from a set of NNW–SSE trending paths crossing the southeastern Superior and passing over the Grenville Front. These data also require a strong low-velocity zone in the mid-upper mantle. However, there is little to distinguish these paths geographically from paths whose velocity-depth profiles are more similar to those of the central Superior, or paths beneath which the apparent lithospheric thickness and velocity is considerably lower than the average for the

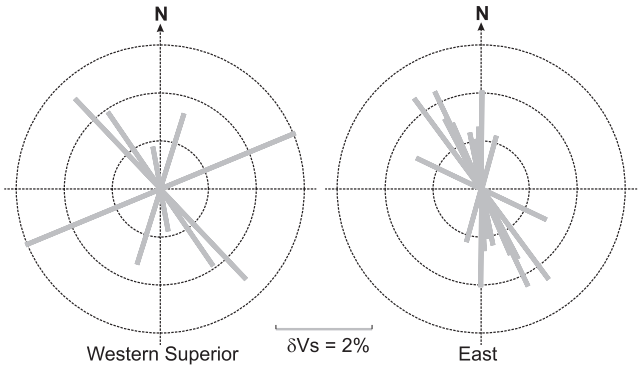

Figure 13. Rose diagrams showing the relationship between the average per cent velocity perturbation above iasp91 in the lithospheric lid and the path azimuth, for paths crossing the western Superior and eastern regions.

region. The seemingly contradictory results for the different paths in this region suggest that the crust and mantle structure is highly heterogeneous, and likely includes complex patterns of anisotropy. In order to resolve these patterns and make sense of the mantle structures, it will be necessary to study the region in considerably more detail, using closely spaced seismograph stations covering the area in an array pattern conducive to a full-3-D investigation.

6.2 Comparison with tomographic studies of other continental cratons

Priestley & Debayle (2003), using fundamental and higher-mode Rayleigh waves to generate a 3-D S_V model of Eurasia, modelled a lithospheric thickness of ∼175–225 km across much of the Siberian craton, though they noted some localized regions where the lithospheric lid may extend to as much as 250 km depth. Multimode 3-D inversions of velocity and anisotropy structure beneath the Australian continent (Debayle & Kennett 2000; Simons *et al.* 2002) indicate an average lithospheric thickness of 225 ± 50 km associated with the Proterozoic-Archean craton. There is evidence for strong complex anisotropy, particularly in the upper 150 km. With the addition of data from new temporary arrays, studies of the western Australian upper mantle in particular have been able to resolve structural variation within individual cratons (Fishwick *et al.* 2005). Significant lateral and vertical wavespeed variations were modelled, indicating a complex cratonic lithospheric structure with no simple relationship to surface geology.

Shear wave velocity beneath southern Africa was studied by Freybourger *et al.* (2001) and Saltzer (2002), who presented average 1-D velocity-depth models for the region. They modelled high velocities to a depth of ∼220 km, with anisotropy through most of the lithospheric section. Priestley & McKenzie (2002) suggested a maximum lithospheric thickness of ∼160 km for the region, but a more recent study (Priestley *et al.* 2006) suggested an average lithospheric thickness of ∼175 km for the southern African cratons, in good agreement with estimates from analysis of kimberlite nodules. Body wave tomography (James *et al.* 2001) indicated thick high-velocity roots under the Archean cratons, extending to at least 200–250 km depth, but little evidence of roots beneath the Proterozoic mobile belts. Some velocity variation (∼0.5 per cent in *P* wavespeed) within the southern African cratons was also resolved. A surface wave study of the Tanzanian craton (Weeraratne *et al.* 2003) modelled high upper-mantle velocities to a depth of ∼140–170 km, with a prominent low-velocity zone beneath the upper mantle 'lid', which they attributed to high temperatures and partial melt associated with a plume head. Surface wave tomography studies by van der Lee *et al.* (2001) indicated the presence of high-velocity lithospheric roots beneath the south American cratons and the intracratonic Amazon Basin, typically extending to depths of ∼150 km, though some cratons appeared to have thinner and slower lithosphere. The results of the study suggested a thinner and/or weaker cratonic lithosphere in south America than that in north America. Bruneton *et al.* (2004) modelled high shear wave velocities in the mantle to a depth of ∼250 km beneath the central Baltic Shield. The study was able to resolve structures to a relatively high lateral resolution (150 km) and indicated significant variations (±3 per cent) in *S*-wavespeed across the study area. The pattern of variation was fairly complex, though some correlation with surface geology was postulated. Archean domains were associated with slower velocities than Proterozoic domains below 100 km depth, in contrast to most other studies of shield regions. The high velocities in the central region were also resolved in body wave tomography studies (Sandoval *et al.* 2004), in which *P* wavespeeds were modelled to vary by up to 4 per cent across the array. A maximum lithospheric thickness of ∼180 km was modelled for south-central Greenland by Darbyshire *et al.* (2004), increasing from ∼100 km near the southeastern coast. The highest lithospheric velocities were associated with a collisional zone between two Archean cratons.

The most detailed studies of other cratons within Canada come from the Slave craton in the Northwest Territories, with investigations using a variety of seismic methods (e.g. Bostock 1998; Snyder *et al.* 2003), magnetotelluric methods (e.g. Jones *et al.* 2003) and geochemical studies (e.g. Kopylova *et al.* 2004). These studies suggest lithospheric thicknesses of ∼200–250 km for the Slave craton, with significant mantle anisotropy.

The velocity models for the Superior Province presented here suggest that the lithosphere of the central and western Superior may be somewhat thinner than the average for continental cratons worldwide. In contrast, the northeastern part of the study area appears to have a lithospheric thickness comparable with the higher end of the global results. The complexity of the models for eastern Ontario makes any comparison difficult, though the predominant values for lithospheric thickness are comparable to the average for continental cratons. The more recent studies discussed above show that, with the increasingly good lateral resolution afforded by surface wave tomography using regional station arrays, it is possible to image seismic velocity variations within individual continental cratons. Significant internal velocity variation and anisotropic structure is apparent in many cases, suggesting that the complexity apparent in the Superior Province is shared by other cratons worldwide.

6.3 Other recent seismic studies of the region

6.3.1 Surface-wave tomography and SKS splitting

Fig. 14 shows a compilation of shear wave splitting results for Ontario and the surrounding region (Frederiksen *et al.* 2006b, and references therein), superimposed on the NA04 shear wave velocity model of van der Lee & Frederiksen (2005), which was derived from partitioned waveform inversion of fundamental and higher mode Rayleigh waves. The shear wave splitting times are shown as black or grey bars whose length is proportional to the delay time and whose orientation indicates the fast direction of anisotropy. The western Superior is characterized by a relatively consistent fast direction and large splitting times of ∼1–2 s. The dominant fast

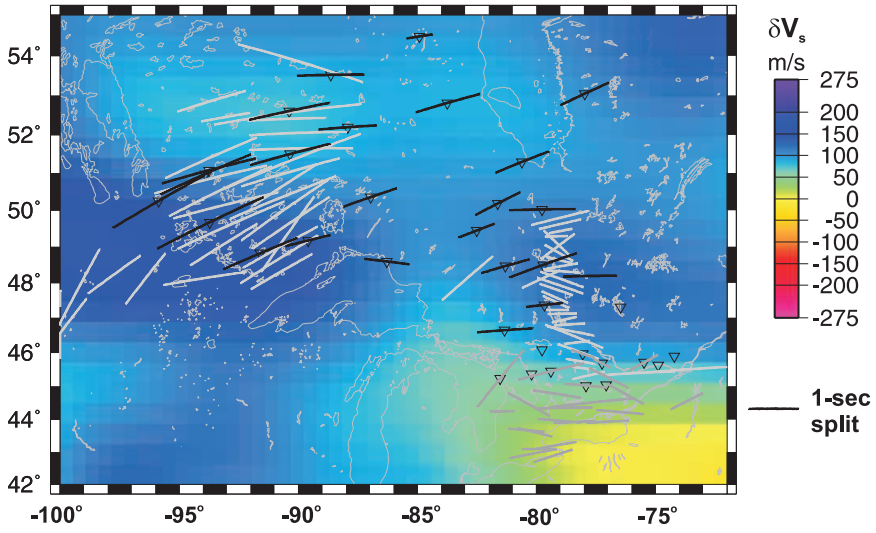

Figure 14. Shear wave splitting results (Frederiksen *et al.* 2006b, and references therein) for the study region, superimposed on the NA04 (van der Lee & Frederiksen 2005) shear wave velocity model at 200 km depth. The velocity perturbations are in m/s from a global reference model. Black bars—shear wave splits from FedNor stations; dark grey bars—splits from POLARIS stations; light grey bars—splits from previous studies using temporary seismograph deployments.

direction lies along the same orientation as the fast surface wave paths observed in this study (e.g. ULM-VIMO), and is the most likely explanation for the anomalously high apparent phase velocities along those paths. In eastern Ontario, inspection of the splitting results for POLARIS, FedNor and previous studies shows a more variable pattern of anisotropy. In general, the splits tend to be smaller than those measured for the western Superior (typically in the range 0.3–1.2 s) with the most common fast direction approximately eastwest, though a large range is apparent, and the split time and fast direction appear to vary over a relatively short distance in some cases. This apparent complexity is consistent with the variability in the velocity-depth models for the eastern Ontario paths.

Inspection of the NA04 surface wave tomography model shows a well-developed high-velocity lid covering the entire study region at 150 km depth. The lid is still pronounced at 200 km depth, but a divot of anomalously low velocity cuts into the lid beneath the far southeast. The divot is more pronounced and more extensive at 250 km depth, but higher than average velocities still cover most of the Superior Province in the region of study. Some internal structure is apparent in the model for the Superior Province lithosphere. However, the lack of station coverage in the region for the NA04 data set means that the interpretation of small-scale features is inappropriate, given that some of the model features may result from variations in ray coverage instead of variations in upper-mantle structure.

The overall pattern of lithospheric thickness and velocity resolved in this study exhibits some similarity with the global shear wave velocity model of Shapiro & Ritzwoller (2002). In the present study, velocities substantially above those of iasp91 are prevalent across the region to a depth of at least ∼150 km, except for an indentation of lower velocities in parts of southeastern Ontario, similar to that resolved in the NA04 model. At 200 km depth, the highest shear wave velocities beneath Ontario and western Quebec are restricted to the northern regions, with lower velocities beneath the southern and southwestern Superior and southern Ontario. At 250 km depth, there is relatively little high-velocity signature beneath Ontario, and lower than average velocities are modelled beneath parts of eastern Ontario/western Quebec.

6.3.2 Crustal thickness variations and relation to upper mantle structure

Substantial variations in apparent crustal thickness, from 32 ± 0.8 km to 48 ± 0.6 km, are evident from the receiver-function analysis. Crustal thickness contours delineate a region of thicker-than-average crust at ∼85°W, extending NNE from Lake Superior towards James Bay. The thinnest crust is inferred to be in the extreme SE corner of the study region around station HSMO. A 50 per cent increase in apparent crustal thickness (16 ± 1.4 km) occurs from station HSMO to station KAPO over a distance of ∼300 km. Since the entire region has an elevation from 200 m to 500 m above sea level, this change in apparent crustal thickness reflects topographic variations for the Moho that are far greater than expected based on simple isostatic considerations.

The thickest crust occurs within the 1.85 Ga Kapuskasing Uplift. Our crustal thickness estimate of 48 ± 0.6 km at KAPO is consistent with Moho depths from crustal refraction profiles across this structure (Percival & West 1994), suggesting that the area of thickened crust may represent preserved ('frozen') Moho topography that originated when the structure was formed as a result of thrust stacking. Other examples of frozen Moho topography have been found in various parts of the Canadian Shield and ancient orogenic belts in other parts of the world, and may be preserved as a result of partial ecologitization of deeply buried lower crustal rocks (Eaton 2006, and references therein). We remark that this broad, NNE-trending Moho structure appears to be unrelated to variations in lithospheric properties from surface-wave analysis. This suggests a degree of decoupling between orogenic and post-orogenic processes at the Moho level from processes that affect the lithospheric mantle.

6.4 Mantle heterogeneity on multiple spatial and temporal scales: evidence from geochemistry

Garnet xenocrysts from kimberlite and alkaline magmatic bodies in the Superior Province were analysed in detail by Scully *et al.* (2004). In eastern Ontario, Mesozoic kimberlites are found in the

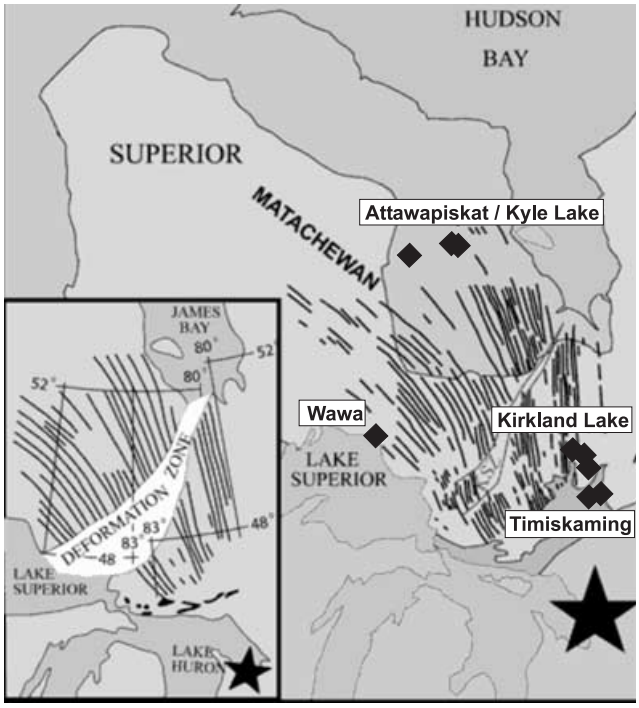

Figure 15. Locations of major features associated with mantle thermal anomalies; the 2490–2450 Ma Matachewan dyke swarm (Ernst & Buchan 2001) and the Attawapiskat/Kyle Lake, Kirkland Lake, Timiskaming and Wawa kimberlite fields (black diamonds; Heaman & Kjarsgaard 2000; Scully *et al.* 2004). The focal point of the dyke swarm is marked with a star. The swarm radiation pattern was disrupted by the younger Kapuskasing Structural Zone (KSZ); a paleomagnetic reconstruction of the pattern is shown in the inset. After Ernst & Buchan (2001).

Attawapiskat, Kirkland Lake and Timiskaming regions, and Proterozoic kimberlites (∼1.14–1.10 Ga) are found in the Kyle Lake and Wawa regions (Fig. 15). Trace-element analysis and geothermometry analysis were carried out on suites of peridotite garnets from each of the pipes in the region. While many of the results were typical of kimberlites found in Archean cratons worldwide, there was significant variation in the garnet compositions, which may be attributed to both spatial and temporal variation in mantle lithosphere composition in the region.

Geothermometry, calibrated using a conductive geotherm typical of cratonic mantle lithosphere and consistent with regional heat flow measurements (Mareschal *et al.* 2000), showed that the garnet suites sampled a wide range of depths within the mantle lithosphere. At Kirkland Lake and Timiskaming, sampling depths ranged from ∼110 to 170–180 km. Deeper sampling was recorded for the Proterozoic pipes at Kyle Lake and Wawa, with maximum depths of ∼200 km.

Rare-earth element signatures from the garnet suites at different Mesozoic kimberlite pipes indicate changes in mantle depletion with depth, from a highly depleted character sampled at ∼100–120 km depth to a composition closer to primitive upper mantle at greater depths. The trend is different at the Proterozoic pipes, with depleted mantle inferred at greater depths. This variation may be interpreted (Scully *et al.* 2004) as a change in mantle composition beneath parts of the Superior Province during the formation of the Midcontinent Rift and associated flood basalt emplacement. The rifting event is approximately contemporaneous with the ages of the Wawa and Kyle Lake kimberlites. In addition, rare-earth element patterns appear to have significant variation between different pipes in the Kirkland Lake and Timiskaming clusters. In particular, differences appear for pipes in locations separated by major faults within the Lake Timiskaming rift system. Scully *et al.* (2004) suggest two possible reasons for these differences: tectonism along the Paleozoic rift system may juxtapose parts of the lithosphere with different chemical signatures, or the passage of the Great Meteor hotspot may have modified the lithospheric composition along relatively narrow zones in the mantle.

The results from the geochemical analysis suggest that the Superior Province upper mantle is highly heterogeneous, with significant compositional variations over relatively small distances. This information may provide some clues as to why the surface wave models are so variable in the eastern region. Some of the length scales described by Scully *et al.* (2004) are too small to be resolved by the surface wave analysis, which samples the average structure both along and either side of an ideal great-circle path, but the complexity may extend to scales that affect the path-averaged results significantly. The resolution in this region is insufficient to resolve the details of localized structure; all that can be stated with confidence is that the area's complexity is not confined to the surface or the crust, but that significant variations in upper-mantle structure appear to exist on relatively small scales.

6.5 Plume and rift influences in eastern Ontario

The influence of plumes/hotspots on the eastern Ontario lithosphere has a history stretching back to at least the Archean/Proterozoic boundary. The 2.45 Ga Matachewan dyke swarm (Ernst & Buchan 2001) outcrops throughout the Superior Province in eastern and central Ontario, and extends well into the region now covered by Phanerozoic sediments (Fig. 15). However, it is not clear what effect the presence of the thermal anomaly that caused the dyke swarm may have had on the mantle lithosphere. Thermal anomalies in the Proterozoic mantle also led to the eruption of kimberlites and lamprophyres in the Attawapiskat and Wawa regions (Scully *et al.* 2004). The passage of the North American continent over the Great Meteor hotspot in Jurassic times led to the eruption of kimberlites at Attawapiskat, Kirkland Lake and Timiskaming (Heaman & Kjarsgaard 2000), but had a more intense effect on the lithosphere further to the southeast, with the eruption of large volumes of material in the Monteregian Hills volcanic province (Sleep 1991). Evidence for anomalous structure in the upper mantle arising from the Great Meteor hotspot is suggested by a linear low-velocity anomaly in body wave tomography models of eastern Ontario and westernmost Quebec (Rondenay *et al.* 2000; Aktas & Eaton 2006), and the low-velocity divot beneath southeastern Ontario, imaged by surface wave tomography (e.g. van der Lee & Frederiksen 2005). The low-velocity anomalies and volcanism may suggest significant erosion of the continental lithosphere by the hotspot; however, the hotspot track also extends through regions where the average present-day lithospheric thickness exceeds 150 km (central-eastern Ontario) or even 200 km (northeastern Ontario). Compositional differences between the lithosphere of the Superior craton and Grenville Province may affect the interaction between the hotspot and the overlying continental lithosphere; however it is also likely that the shape of the thick Superior cratonic keel had a significant influence on the hot plume material, deflecting it towards regions of thinner lithosphere (e.g. Sleep *et al.* 2002).

Surface wave paths crossing Lake Superior (e.g. BUKO-ATKO, SUNO-ATKO; see Fig. 1 for locations) all show lower than average

phase velocities at intermediate periods (typically ∼70–120 s). This result suggests that there may be anomalously low shear wave velocity in the mid-upper mantle beneath Lake Superior, which may be attributed to thermal or compositional alteration as a result of the Keweenawan Mid-continent rifting event. The rift region is also characterized by thickened crust (Fig. 11). The main arm of the rift arcs beneath Lake Superior (e.g. Thurston *et al.* 1991), with related outcrops in the Lake Nipigon region.

7 CONCLUSIONS

(i) The Superior Province, the world's largest Archean craton, is underlain by lithospheric mantle that exhibits strong regional variations in anisotropy and velocity structure; thus, there is not a single standard 'Canadian Shield' model for the lithosphere that is universally applicable to this craton.

(ii) The lithospheric thickness inferred from inversion of Rayleigh wave dispersion curves varies from ∼140 km to ∼240 km across most of the province.

(iii) In the western Superior craton, the inferred fast propagation direction for Rayleigh waves is consistent with the ENE-WSW fast direction found from *SKS* splitting.

(iv) *S*-wave velocities in the Superior mantle lid appear to vary from ∼2 per cent to >6 per cent higher than the iasp91 reference model. Since the paths used in two-station surface-wave inversions contain a range of azimuths, the observed scatter in apparent velocities may be partly due to seismic anisotropy.

(v) Crustal thickness inferred from teleseismic receiver functions varies between 32 and 48 km. Areas of greater than average crustal thickness occur beneath the Mesoproterozoic Mid-continent Rift and Paleoproterozoic Kapuskasing Uplift.

(vi) The lithospheric structure of the southeastern Superior craton is complex and incompletely resolved by the available data. This region was influenced by mantle plume events, as manifested in the 2.45 Ga Matachewan dyke swarm and the Mesozoic Attawapiskat—Kirkland Lake—Timiskaming kimberlite trend. This association suggests that mantle plumes played a significant role in modifying the lithospheric root beneath parts of the Superior craton.

(vii) There are significant differences in the inferred orientation and location of mantle domain boundaries compared to structures at the Moho level. This suggests a degree of decoupling between orogenic and post-orogenic processes at the Moho level from processes that affect that deeper lithospheric mantle.

ACKNOWLEDGMENTS

The installation and operation of the broad-band seismograph network in southern Ontario and surrounding regions was funded by the Canada Foundation for Innovation, the Ontario Innovation Trust Fund, the Natural Sciences and Engineering Research Council of Canada and Ontario Power Generation. Funding for northern Ontario seismograph stations was provided by the Federal Economic Development Initiative for Northern Ontario (FedNor).

FD is a post-doctoral fellow at UWO and visiting scientist at the Geological Survey of Canada, funded by Ontario Challenge Fund project #01-Mar-0906.

We thank all staff and students involved with the deployment and maintenance of the seismic array; in particular, Isa Asudeh (Geological Survey of Canada) for his coordination of the projects.

Local contacts at the station sites are essential to the success of the project. We thank all for their help and cooperation, including university researchers, mine owners, private landowners, businesses, municipal and provincial authorities, and First Nations Band councils.

This manuscript benefitted from useful discussions with Desmond Moser, David Snyder, Tom Skulski and Don White, and from constructive reviews by Jeannot Trampert, Helle Pedersen and Sergei Lebedev.

GSC Contribution Number: 20060055.

REFERENCES

Adams, J. & Basham, P., 1991. The seismicity and seismotectonics of eastern Canada, in *Neotectonics of North America,* Geological Society of America Decade map, Vol. 1, pp. 261–276, eds Slemmons, D.B., Engdahl, E.R., Zoback, M.D. & Blackwell, D.D., Boulder, Colorado.

Aktas, K. & Eaton, D.W., 2006. Upper-mantle velocity structure of the lower Great Lakes region. *Tectonophysics,* **420,** 267–281.

Bokelmann, G.H.R. & Silver, P.G., 2000. Mantle variation within the Canadian Shield: travel times from the portable broadband Archean-Proterozoic Transect 1989, *J. geophys. Res.,* **105,** 579–605.

Boland, A.V. & Ellis, R.M., 1989. Velocity structure of the Kapuskasing uplift, northern Ontario, from seismic refraction studies, *J. geophys. Res.,* **94,** 7189–7204.

Bostock, M., 1998. Seismic stratigraphy and evolution of the Slave province, *J. geophys. Res.,* **103,** 21 183–21 200.

Bostock, M.G. & Cassidy, J.F., 1995. The upper mantle discontinuities in western Canada from Ps conversions, *Pure appl. Geophys.,* **145,** 219–234.

Brune, J. & Dorman, J., 1963. Seismic waves and earth structure in the Canadian Shield, *Bull. seism. Soc. Am.,* **53,** 167–210.

Bruneton, M. *et al.*, 2004. Complex lithospheric structure under the central Baltic Shield from surface wave tomography, *J. geophys. Res.,* **109,** B10303, doi:10.1029/2003JB002947.

Calvert, A.J., Sawyer, E.W., Davis, W.J. & Ludden, J.N., 1995. Archaean subduction inferred from seismic images of a mantle suture in the Superior Province, *Nature,* **375,** 670–674.

Carlson, R.W., Pearson, D.G. & James, D.E., 2005. Physical, chemical and chronological characteristics of continental mantle, *Rev. Geophys.,* **42,** 1–24.

Cotte, N., Pedersen, H.A., Campillo, M., Farra, V. & Cansi, Y., 2000. Off-great circle propagation of intermediate-period surface waves observed on a dense array in the French Alps, *Geophys. J. Int.,* **142,** 825–840.

Crough, S.T., 1981. Mesozoic hotspot epeirogeny in eastern North America, *Geology,* **9,** 2–6.

Darbyshire, F.A. & Asudeh, I., 2006. Generic instrument responses for the POLARIS and FedNor seismograph network in Canada, *Geological Survey of Canada Open File,* **5185,** 23pp.

Darbyshire, F.A. *et al.*, 2004. A first detailed look at the Greenland lithosphere and upper mantle, using Rayleigh wave tomography, *Geophys. J. Int.,* **158,** 267–286.

Davidson, A., 1996. The Mesoproterozoic Grenville orogen, in *Searching for diamonds in Canada, Geological Survey of Canada Open File,* Vol. 3228, pp. 25–27. eds LeCheminant, A.N., Richardson, D.G., DiLabio, R.N.W. & Richardson, K.A., Geol. Survey Canada, Ottawa, Canada.

Debayle, E. & Kennett, B.L.N., 2000. The Australian continental upper mantle: Structure and deformation inferred from surface waves, *J. geophys. Res.,* **105,** 25 423–25 450.

Eaton, D., 2006. Multi-genetic origin of the continental Moho: insights from LITHOPROBE. *TerraNova,* **18,** 34–43. doi:10.1111/j.1365-3121.2005.00657.x

Eaton, D., Frederiksen, A. & Miong, S.-K., 2004. Shear-wave splitting observations in the lower Great Lakes region; evidence for regional anisotropic domains and keel-modified asthenospheric flow, *Geophys. Res. Lett.,* **31**: doi:10.1029/2004GL019438.

Eaton, D. *et al.*, 2005. Investigating Canada's Lithosphere and Earthquake Hazards with Portable Arrays, *EOS, Trans. Am. geophys. Un.,* **86**(17), 169–176.

Eaton, D.W., Dineva, S. & Mereu, R., 2006. Crustal thickness and Vp/Vs variations in the Grenville orogen (Ontario, Canada) from analysis of teleseismic receiver functions, *Tectonophysics,* **420,** 223–238.

Ernst, R.E. & Buchan, K.L., 2001. The use of mafic dyke swarms in identifying and locating mantle plumes, in *Mantle Plumes: Their Identification Through Time,* Vol. 352, pp. 247–265, eds Ernst, R.E. & Buchan, K.L., Geol. Soc. Am. Spec. Paper.

Fishwick, S., Kennett, B.L.N. & Reading, A.M., 2005. Contrasts in lithospheric structure within the Australian craton—insights from surface wave tomography, *Earth planet. Sci. Lett.,* **231,** 163–176.

Ferguson, I.J. *et al.*, 2005. Geoelectric response of Archean lithosphere in the western Superior Province, central Canada, *Phys. Earth planet. Inter.,* **150,** 123–143.

Forte, A.M. & Perry, H.K.C., 2000. Geodynamic evidence for a chemically depleted continental tectosphere, *Science,* **290,** 1940–1944.

Frederiksen, A.W., Bostock, M.G. & Cassidy, J.F., 2001. S-wave velocity structure of the Canadian upper mantle, *Phys. Earth planet. Inter.,* **124,** 175–191.

Frederiksen, A.W., Ferguson, I.J., Eaton, D., Miong, S.-K. & Gowan, E., 2006a. Mantle fabric at multiple scales across an Archean-Proterozoic boundary, Grenville Front, Canada, *Phys. Earth planet. Inter.,* **158,** 240–263.

Frederiksen, A.W., Miong, S.-K., Darbyshire, F., Eaton, D., Rondenay, S. & Sol, S., 2006b. Lithospheric Variations Across the Superior Province, Ontario, Canada: Evidence from Tomography and Shear-Wave Splitting, *J. geophys. Res.,* submitted.

Freybourger, M., Gaherty, J.B. & Jordan, T.H., 2001. Structure of the Kaapvaal Craton from surface waves, *Geophys. Res. Lett.,* **28,** 2489–2492.

Godey, S., Deschamps, F. & Trampert, J., 2004. Thermal and compositional anomalies beneath the North American continent, *J. geophys. Res.,* **109,** B01308, doi:10.1029/2002JB002263.

Gomberg, J.S., Priestley, K.F., Masters, T.G. & Brune, J.N., 1988. The structure of the crust and upper mantle of northern Mexico, *Geophys. J.,* **94,** 1–20.

Grand, S.P., 1994. Mantle shear structure beneath the Americas and surrounding oceans, *J. geophys. Res.,* **99,** 11 591–11 621.

Griffin, W.L., O'Reilly, S.Y. & Ryan, C.G., 1999. The composition and origin of subcontinental lithospheric mantle, in *Mantle Petrology; Field Observations and High-Pressure Experimentation; A Tribute to Francis R. Boyd, J.,* Vol. 6, pp. 13–45, eds Fei, Y., Bertka, C., Mysen, M. & Bjorn, O., Special Publication, Geochemical Society.

Gung, Y., Panning, M. & Romanowicz, B., 2003. Global anisotropy and the thickness of continents, *Nature,* **422,** 707–711.

Heaman, L.M. & Kjarsgaard, B.A., 2000. Timing of eastern North American kimberlite magmatism: continental extension of the Great Meteor hotspot track?, *Earth planet. Sci. Lett.,* **178,** 253–268.

Herrmann, R.B. & Ammon, C.J., 2002. *Computer programs in Seismology: Surface Waves, Receiver Functions and Crustal Structure,* Vol. 3.20., St. Louis University.

Hoffman, P.F., 1988. United Plates of America, the birth of a craton: early Proterozoic assembly and growth of Laurentia, *Annu. Rev. Earth Planet. Sci.,* **16,** 543–603.

Holbrook, W.S., Mooney, W.D. & Christensen, N.I., 1992. The seismic velocity structure of the deep continental crust, in *Continental Lower Crust,* pp. 1–44, eds Fountain, D.M., Arculus, R. & Kay, R.W., Elsevier, Amsterdam.

James, D.E., Fouch, M.J., VanDecar, J.C., van der Lee, S. & Kaapvaal Seismic Group, 2001. Tectospheric structure beneath southern Africa, *Geophys. Res. Lett.,* **28,** 2485–2488.

Jones, A.G., Lezaeta, P., Ferguson, I.J., Chave, A.D., Evans, R.L., Garcia, X. & Spratt, J., 2003. The electrical structure of the Slave craton, *Lithos,* **71,** 505–527.

Jordan, T.H., 1975. The continental tectosphere, *Rev. Geophys.,* **13,** 1–12.

Kamo, S.L., Krogh, T.E. & Kumarapeli, P.S., 1995. Age of the Grenville dyke swarm, Ontario-Quebec: implications for the timing of Iapetan rifting, *Can. J. Earth Sci.,* **32,** 273–280.

Kay, I., Sol, S., Kendall, J-M., Thomson, C., White, D., Asudeh, I., Roberts, B. & Francis, D., 1999a. Shear wave splitting observations in the Archean craton of Western Superior, *Geophys. Res. Lett.,* **26,** 2669–2672.

Kay, I. *et al.*, 1999b. Imaging the Moho and Vp/Vs ratio in the Western Superior Archean Craton with wide-angle reflections, *Geophys. Res. Lett.,* **26,** 2585–2588; doi:10.1029/1999Gl010422.

Kendall, J-M., Sol, S., Thomson, C.J., White, D.E., Asudeh, I., Snell, C.S. & Sutherland, F.H., 2002. Seismic heterogeneity and anisotropy in the Superior Province, Canada: Insights into the evolution of an Archaean craton, in *The Early Earth: Physical, Chemical and Biological Development,* Vol. 199, pp. 27–44, eds Fowler, C.M.R., Ebinger, C.J. & Hawkesworth, C.J., Geol. Soc. London, Spec. Pub.

Kennett, B.L.N. & Engdahl, E.R., 1991. Traveltimes for global earthquake location and phase identification, *Geophys. J. Int.,* **105,** 429–465.

Kopylova, M.G., Lo, J. & Christensen, N.I., 2004. Petrological constraints on seismic properties of the Slave upper mantle (northern Canada), *Lithos,* **77,** 493–510.

Langston, C.A., 1977. The effect of planar dipping structure on source and receiver responses for constant ray parameter, *Bull. seism. Soc. Am.,* **67,** 1029–1050.

Li, X.D. & Romanowicz, B., 1996. Global mantle shear velocity model developed using nonlinear asymptotic coupling theory, *J. geophys. Res.,* **101,** 22 245–22 272.

Ludden, J. & Hynes, A., 2000. The Lithoprobe Abitibi-Grenville transect: two billion years of crust formation and recycling in the Precambrian Shield of Canada, *Can. J. Earth Sci.,* **37,** 459–476.

Mareschal, J.C., Jaupart, C., Gariépy, C., Cheng, L.Z., Guillou-Frottier, L., Bienfait, G. & Lapointe, R., 2000. Heat flow and deep thermal structure near the southeastern edge of the Canadian Shield, *Can. J. Earth Sci.,* **37,** 399–414.

Masters, G., Johnson, S., Laske, G. & Bolton, H., 1996. A shear-velocity model of the mantle, *Phil. Trans. R. Soc. Lond.,* **354,** 1385–1411.

Maupin, V. & Cara, M., 1992. Love-Rayleigh wave incompatibility and possible deep upper mantle anisotropy in the Iberian Peninsula, *Pure. appl. Geophys.,* **138,** 429–444.

Megnin, C. & Romanowicz, B., 2000. The three-dimensional shear velocity structure of the mantle from the inversion of body, surface and higher-mode waveforms, *Geophys. J. Int.,* **143,** 709–728.

Musacchio, G., White, D.J., Asudeh, I. & Thomson, C.J., 2004. Lithospheric structure and composition of the Archean western Superior Province from seismic refraction/wide-angle reflection and gravity modeling, *J. geophys. Res.,* **109,** B03304, doi:10.1029/2003JB002427.

Nelson, K.D., 1991. A unified view of craton evolution motivated by recent deep seismic reflection and refraction results, *Geophys. J. Int.,* **105,** 25–35.

Nettles, M. & Dziewonski, A.M., 2004. Advances in global and regional tomography using the GSN, *EOS, Trans. Am. geophys. Un.,* **85**(17), *Jt. Assem. Suppl.*, Abstract S44A-02.

Nitescu, B., Cruden, A.R. & Bailey, R.C., 2006. Crustal structure and implications for the tectonic evolution of the Archean Western Superior craton from forward and inverse gravity modelling, *Tectonics,* **25,** TC1009, doi: 10.1029/2004TC001717.

Owens, T.J., Zandt, G. & Taylor, S.R., 1984. Seismic evidence for an ancient rift beneath the Cumberland Plateau, Tennessee: A detailed analysis of broadband teleseismic P waveforms, *J. geophys. Res.,* **89,** 7783–7795.

Pearson, D.G., 1999. Evolution of cratonic lithospheric mantle: an isotopic perspective, in *Mantle Petrology; Field Observations and High-Pressure Experimentation; A Tribute to Francis R. Boyd, J.,* Vol. 6, pp. 57–78, eds Fei, Y., Bertka, C., Mysen, M. & Bjorn, O., Special Publication, Geochemical Society.

Pedersen, H.A., 2006. Impacts of non-plane waves on two-station measurements of phase velocities, *Geophys. J. Int.,* **165,** 279–287.

Pedersen, H.A., Coutant, O., Deschamps, A., Soulage, M. & Cotte, N., 2003. Measuring surface wave phase velocities beneath small broad-band arrays: tests of an improved algorithm and application to the French Alps, *Geophys. J. Int.,* **154,** 903–912.

Percival, J.A., 1996. Archean cratons, in *Searching for diamonds in Canada, Geological Survey of Canada Open File,* Vol. 3228, pp. 11–15, eds

LeCheminant, A.N., Richardson, D.G., DiLabio, R.N.W. & Richardson, K.A.
Percival, J.A. & West, G.F., 1994. The Kapuskasing Uplift: a geological and geophysical synthesis, *Can. J. Earth Sci.,* **31,** 1256–1286.
Perry, H.K.C., Eaton, D.W.S. & Forte, A.M., 2002. LITH5.0: a revised crustal model for Canada based on Lithoprobe results, *Geophys. J. Int.,* **150,** 285–294.
Priestley, K. & McKenzie, D., 2002. The structure of the upper mantle beneath southern Africa, in *The early Earth: physical, chemical and biological development, Geol. Soc. London, Spec. Pub,* Vol. 199, pp. 27–44, eds Fowler, C.M.R., Ebinger, C.J. & Hawkesworth, C.J.
Priestley, K. & Debayle, E., 2003. Seismic evidence for a moderately thick lithosphere beneath the Siberian Platform, *Geophys. Res. Lett.,* **30,** 1118, doi:10.1029/2002GL015923.
Priestley, K., McKenzie, D. & Debayle, E., 2006. The state of the upper mantle beneath southern Africa, *Tectonophysics,* **416,** 101–112.
Ritsema, J., van Heijst, H.J. & Woodhouse, J.H., 2004. Global transition zone tomography, *J. geophys. Res.,* **109,** B02302, doi:10.1029/2003JB002610.
Rivers, T., 1997. Lithotectonic elements of the Grenville Province: review and tectonic implications, *Precambrian Res.,* **86,** 117–154.
Rondenay, S., Bostock, M.G., Hearn, T., White, D.J., Wu, H., Senechal, G., Ji, S. & Mareschal, M., 2000a. Teleseismic studies of the lithosphere below the Abitibi-Grenville Lithoprobe transect, *Can. J. Earth Sci.,* **37,** 415–426.
Rondenay, S., Bostock, M.G., Hearn, T.M., White, D.J. & Ellis, R.M., 2000b. Lithospheric assembly and modification of the SE Canadian Shield: Abitibi-Grenville Teleseismic Experiment, *J. geophys. Res.,* **105,** 13,735–13,754.
Saltzer, R.L., 2002. Upper mantle structure of the Kaapvaal Craton from surface wave analysis: a second look, *Geophys. Res. Lett.,* **29,** doi:10.1029/2001GL013702.
Sandoval, S., Kissling, E., Ansorge, J. & the SVEKALAPKO Seismic Tomography Working Group, 2004. High-resolution body wave tomography beneath the SVEKALAPKO array—II. Anomalous upper mantle structure beneath the central Baltic Shield, *Geophys. J. Int.,* **157,** 200–214.
Scully, K.R., Canil, D. & Schulze, D.J., 2004. The lithospheric mantle of the Archean Superior Province as imaged by garnet xenocryst geochemistry, *Chemical Geology,* **207,** 189–221.
Shapiro, N.M. & Ritzwoller, M.H., 2002. Monte-Carlo inversion for a global shear-velocity model of the crust and upper mantle, *Geophys. J. Int.,* **151,** 88–105.
Shapiro, N.M., Campillo, M., Paul, A., Singh, S.K., Jongmans, D. & Sánchez-Sesma, F.J., 1997. Surface-wave propagation across the Mexican Volcanic Belt and the origin of the long-period seismic-wave amplification in the Valley of Mexico, *Geophys. J. Int.,* **128,** 151–166.
Silver, P.G. & Kaneshima, S., 1993. Constraints on mantle anisotropy beneath Precambrian North America from a transportable teleseismic experiment, *Geophys. Res. Lett.,* **20,** 1127–1130.
Silver, P.G., Meyer, R.P. & James, D.E., 1993. Intermediate-scale observations of the Earth's deep interior from the APT89 transportable teleseismic experiment, *Geophys. Res. Lett.,* **20,** 1123–1126.
Simons, F.J., van der Hilst, R.D., Montagner, J-P. & Zielhuis, A., 2002. Multimode Rayleigh wave inversion for heterogeneity and azimuthal anisotropy of the Australian upper mantle, *Geophys. J. Int.,* **151,** 738–754.
Sleep, N.H., 1990. Monteregian hotspot track: A long-lived mantle plume, *J. geophys. Res.,* **95,** 21 983–21 990.
Sleep, N.H., Ebinger, C.J. & Kendall, J.-M., 2002. Deflection of mantle plume material by cratonic keels, in *The Early Earth: Physical, Chemical and Biological Development,* Vol. 199, pp. 27–44, eds Fowler, C.M.R., Ebinger, C.J. & Hawkesworth, C.J., Geol. Soc. London, Spec. Pub.
Snyder, D., Bostock, M. & Lockhart, G., 2003. Two anisotropic layers in the Slave craton, *Lithos,* **71,** 529–539.
Sol, S., 2003. Teleseismic waveform analysis and velocity structure beneath the Western Superior Province: glimpses into the deeper architecture of an Archean craton, *PhD thesis*, Queen's University, Canada.
Sol, S., Thomson, C.J., Kendall, J-M., White, D., Vandecar, J.C. & Asudeh, I., 2002. Seismic tomographic images of the cratonic upper mantle beneath the Western Superior Province of the Canadian Shield—A remnant Archean slab? *Phys. Earth planet. Inter.,* **134,** 53–70.
Su, W.J. & Dziewonski, A.M., 1994. Degree 12 model of shear velocity in the mantle, *J. geophys. Res.,* **99,** 6945–6980.
Thompson, R.N. & Gibson, S.A., 1991. Subcontinental mantle plumes, hotspots and pre-existing thinspots, *J. Geol. Soc. Lond.,* **148,** 973–977.
Thurston, P.C., Williams, H.R., Sutcliffe, R.H. & Stott, G.M. (eds.), 1991. *Geology of Ontario. Ontario Geological Survey Special,* Vol. 4.
van der Lee, S. & Nolet, G., 1997. Upper mantle S-velocity structure of North America, *J. geophys. Res.,* **102,** 22 815–22 838.
van der Lee, S. & Frederiksen, A., 2005, Surface wave tomography applied to the North American upper mantle, in *Seismic Data Analysis and Imaging With Global and Local Arrays, Geophysical Monograph,* Vol. 157, pp. 67–80, eds Nolet, G. & Levander, A., AGU, Washington, DC, USA.
van der Lee, S., James, D. & Silver, P., 2001, Upper mantle S-velocity structure of western and central South America, *J. geophys. Res.,* **106,** 30821–30834.
van Heijst, H.J., Snieder, R. & Nowack, R., 1994. Resolving a low-velocity zone with surface-wave data, *Geophys. J. Int.,* **118,** 333–343.
Weeraratne, D.S., Forsyth, D.W. & Fischer, K.M., 2003. Evidence for an upper mantle plume beneath the Tanzanian craton from Rayleigh wave tomography, *J. geophys. Res.,* **108,** doi:10.1029/2002JB002273.
Wessel, P. & Smith, W.H.F., 1991. Free software helps map and display data, *EOS, Trans. Am. geophys. Un.,* **72,** 441; 445–446.
Wickens, A.J., 1971. Variations in lithospheric thickness in Canada, *Can. J. Earth Sci.,* **8,** 1154–1162.
Zandt, G. & Ammon, C.J., 1995. Continental-crust composition constrained by measurements of crustal Poisson's Ratio, *Nature,* **374,** 152–154.
Zandt, G., Myers, S.C. & Wallace, T.C., 1995. Crust and mantle structure across the Basin and Range—Colorado Plateau boundary at 37°N latitude and implications for Cenozoic extensional mechanism, *J. geophys. Res.,* **100,** 10 529–10 548.
Zhu, H. & Kanamori, H., 2000. Moho depth variation in southern California from teleseismic receiver functions, *J. geophys. Res.,* **105,** 2969–2980.

APPENDIX A: WAVEFRONT PROPAGATION CONSIDERATIONS AND TWO-STATION DISPERSION CURVES

When carrying out measurements of surface wave phase velocity using a two-station method, a number of factors must be taken into account when considering the reliability of the resulting dispersion curves and the magnitude of errors. A number of authors have considered the issue (Pedersen 2006, and references therein) and attempted to quantify the reliability of the measurements. In particular, the effects of non-plane wave contributions, and deviations from the expected great-circle path are important. In each case, errors or systematic bias in the dispersion measurements can be reduced by using multiple events to calculate the dispersion curves. It is important that these events come from several different epicentral regions, and desirable to include reciprocal paths (i.e. events arriving at the network from opposite directions).

Table A1 shows a list of the two-station paths for which modelling for velocity structure was carried out. We indicate the interstation distance, the number of events used in the calculation of the dispersion curves, and the event characteristics. The paths were chosen for velocity modelling for their range of locations (spanning the entire study region), azimuths and profile lengths. There is considerable variation in the availability of events from the correct backazimuths, due to global seismicity patterns, and in the recording duration of the stations in the network. In some cases, the number of events used to calculate the dispersion curves is, therefore, less than optimal.

Table A1. Event distribution for the dispersion curves modelled in this study. 'Reciprocal paths' indicates incoming events from opposite directions. We consider the epicentral distance from the source to the midpoint of the two-station path; different 'epicentral regions' refer to epicentral distance differences of more than 10°.

Path	Interstation distance (km)	Number of events used	Number of different epicentral regions	Reciprocal paths?
Abitibi-north	540	7	4	Y
Abitibi-south	520	19	8	Y
KAPO-south	470	15	6	Y
KILO-south	400	10	4	Y
MALO-south	530	8	6	Y
OTRO-south	610	16	7	Y
RSPO-east	380	9	4	N
SUNO-east	510	5	3	N
VIMO-south	930	17	9	Y
ATKO-PKLO	310	3	2	Y
GAC-PNPO	880	2	2	N
KAPO-PKLO	600	4	3	Y
KAPO-TOBO	480	8	5	Y
KILO-PNPO	480	3	2	N
LDIO-PKLO	260	5	3	Y
MALO-RSPO	440	5	2	N
MALO-SILO	610	13	4	Y
MALO-TOBO	550	9	4	Y
MUMO-PNPO	530	14	7	Y
OTRO-PKLO	630	5	2	N
OTRO-SUNO	390	4	3	Y
PKLO-PNPO	430	11	4	Y
SUNO-ATKO	810	3	2	N
SUNO-PKLO	850	10	5	N
TOBO-PNPO	520	10	6	Y
ULM-PNPO	720	2	2	N
ULM-VIMO	890	10	3	N
VIMO-PNPO	500	3	3	Y

However, all paths use events from at least two different epicentral regions, in order to reduce systematic errors arising from off-great-circle propagation. Tests on subsets of relatively large data sets (e.g. paths such as MALO-SILO and MUMO-PNPO) showed that the averaged dispersion curves did not change significantly with the addition of larger numbers of events, except for the case in which the subset consisted of a group of events very closely spaced in both time and epicentral region (e.g. the Japanese earthquakes of September 5–10 2004).

Pedersen (2006) showed that the adverse effects of non-plane wave energy on interstation phase velocity measurements decrease with increasing profile length. The synthetic tests suggested that calculations for a 400 km interstation path would yield meaningful results with small errors for just a few independent events. At shorter distances the impact of non-plane wave energy was much more significant, due to the fact that the wavelength and the interstation distance become comparable at periods of interest to the structural studies. With the exception of paths ATKO-PKLO (310 km) and LDIO-PKLO (260 km), all the paths studied here have interstation distances close to, or greater than, 400 km. It is unlikely that non-plane wave energy will have a significant effect on the average velocities and error estimates for the majority of the dispersion curves. In contrast, the effects of off-great-circle propagation are independent of profile length.

Deviations from the expected backazimuths of the incoming waves may be quantified using array-based measurements (e.g. Cotte *et al.* 2000). The station spacing and recording time of the northern Ontario seismic network was insufficient to allow reliable dispersion measurements based on array analysis methods, but we were able to measure the backazimuths of a number of incoming events at a four-station array (KILO, OTRO, MALO and KAPO in eastern Ontario) using the method of Pedersen *et al.* (2003). We found that the deviations from the expected great-circle paths were generally smaller than 10° for the period range in which we had obtained stable results using two-station calculations.

The final set of 28 dispersion curves is shown in Figs A1 and A2. The error bars shown in the figures are those used for the Monte-Carlo modelling scheme.

SUPPLEMENTARY MATERIAL

The following supplementary material is available for this article:

Table S1. Events used in receiver function analysis.
Table S2. Events used in surface wave analysis.

This material is available as part of the online article from: http://www.blackwell-synergy.com/doi/abs/10.1111/j.1365-246X.2006.03259.x (this link will take you to the article abstract).

Please note: Blackwell Publishing are not responsible for the content or functionality of any supplementary materials supplied by the authors. Any queries (other than missing material) should be directed to the corresponding author for the article.

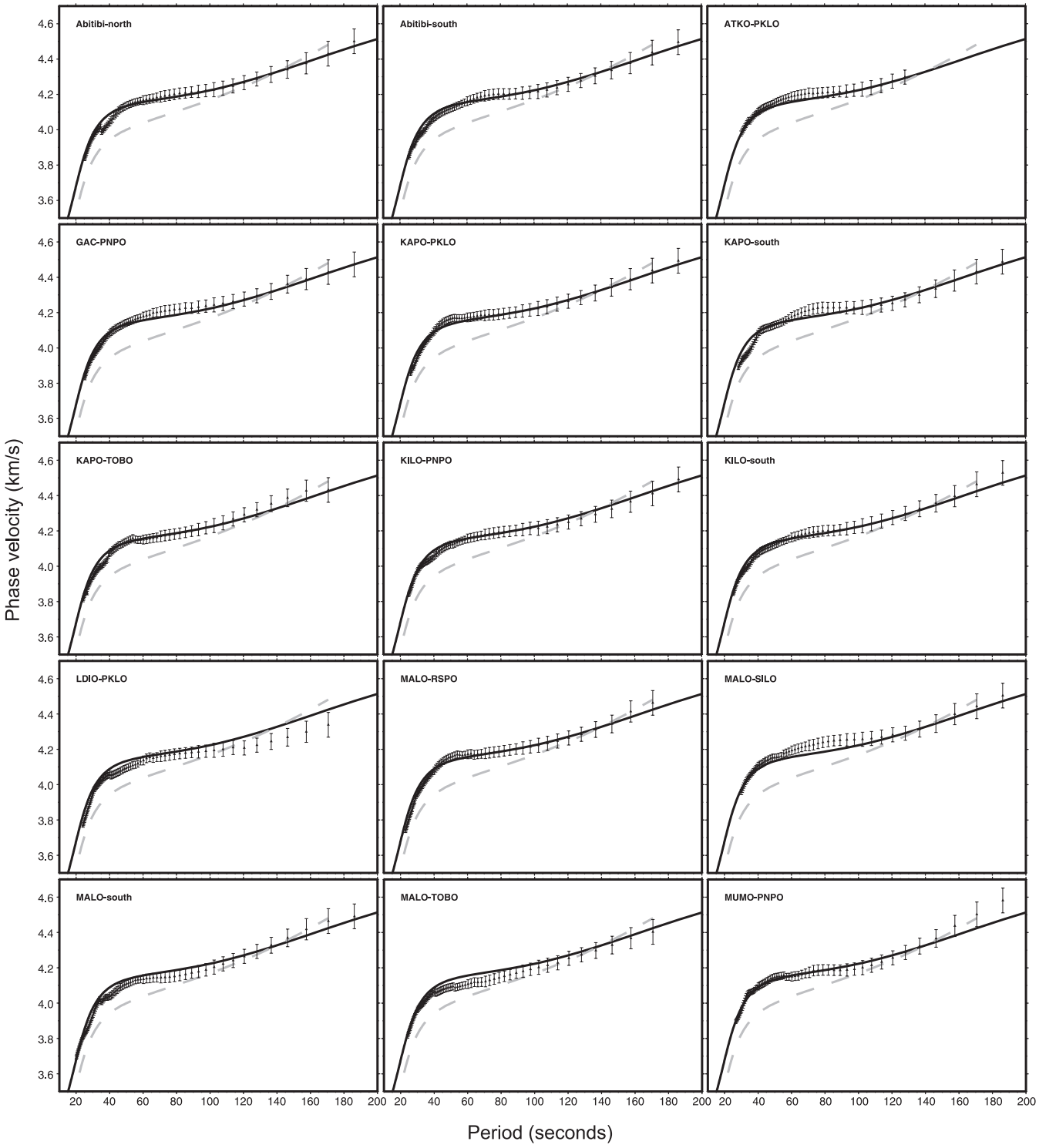

Figure A1. Dispersion curves for 15 interstation paths from which mantle velocity models are derived. Solid line: Dispersion curve for 'CANSD' model (Brune & Dorman 1963); dashed line: dispersion curve for iasp91 global reference model (Kennett & Engdahl 1991). Error bars are those used in the Monte-Carlo modelling procedure.

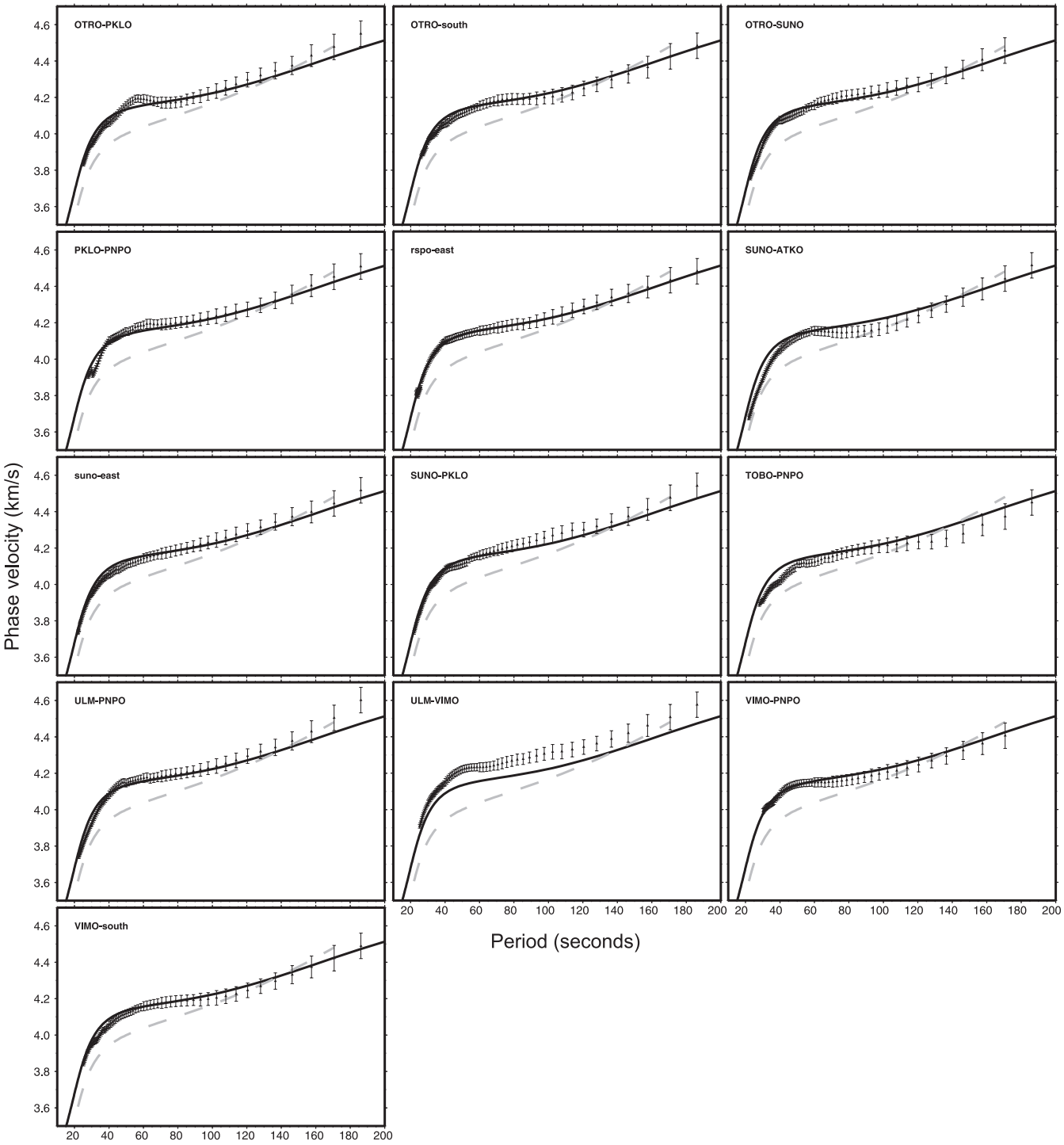

Figure A2. Dispersion curves for the remaining 13 interstation paths from which mantle velocity models are derived.